9

Nonlinear Analysis of Physiological Control Systems

9.1 NONLINEAR VERSUS LINEAR CLOSED-LOOP SYSTEMS

Thus far, the methods we have employed to analyze the dynamics of physiological control systems have been primarily linear methods, although it is clear that nonlinearity is the rule and not the exception in biology. As a first approximation, linear models work surprisingly well in many instances, but one can find many more instances in which the nonlinear features are critical for the functioning of the system in question. Classic examples of this include the mechanism through which the nerve action potential is generated, as modeled by the Hodgkin–Huxley equations, and various phenomena associated with nonlinear oscillators, such as frequency entrainment and phase resetting. These will be discussed in detail later.

A key disadvantage in the analysis of nonlinear systems is that the principle of superposition can no longer be applied. This has profound consequences, for it means that in contrast to linear systems, where the dynamics can be fully characterized in terms of the impulse response, the same concise means of description cannot be applied to the nonlinear system. Another consequence of the inapplicability of the superposition principle is that local solutions cannot be extrapolated to the global scale. As an example, consider the comparison of the linear lung mechanics model described previously (in Chapters 4 and 5) with a version that contains nonlinear feedback. Both models are illustrated in Figure 9.1. The responses of the linear and nonlinear models to input steps in P_{ao} are displayed in Figures 9.2a and 9.2b, respectively. In each case, the responses in P_A to step inputs of amplitude 1 and 2 mm Hg in P_{ao} (starting at time 0.5 s) are shown as the light and bold tracings, respectively. In the linear case, the response to a step input that is twice as large leads to a proportionately scaled version of the response to the unit step. However, in the nonlinear case, the steady-state response to the larger step is clearly less than twice the steady-state response to the unit step in P_{ao}. Furthermore, the response to the larger step is more oscillatory than the unit step response. Thus, knowing the unit impulse response or unit step response of the nonlinear system does not enable us to predict the responses to input steps of other amplitudes.

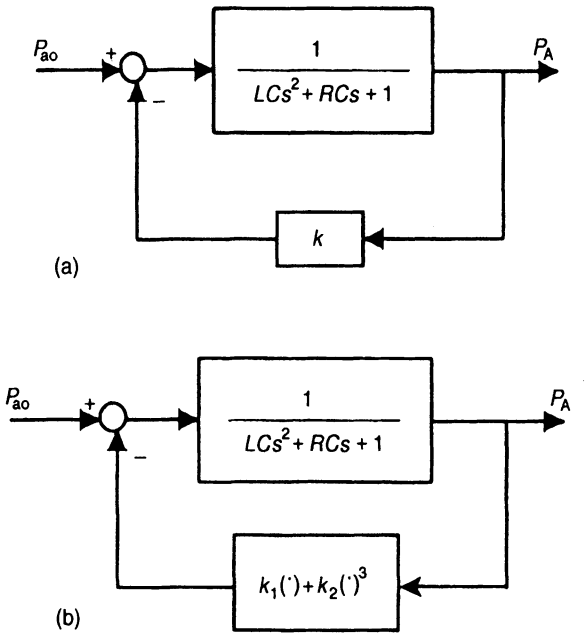

Figure 9.1 (a) Linear lung mechanics model. (b) Lung mechanics model with nonlinear feedback.

There is another major difference between the dynamics of linear and nonlinear systems. As one might recall from Chapter 5, the dynamics of linear systems can also be characterized in terms of their frequency responses, since sinusoidal perturbation of a linear system results in a sinusoidal output of the same frequency. In nonlinear systems, however, sinusoidal perturbation can give rise to a response that contains not only the fundamental frequency of the perturbation but also higher harmonics of that frequency. Figure 9.3 shows a comparison between responses elicited from the linear and nonlinear versions of the lung mechanics model displayed in Figure 9.1. The linear response to an input sine wave of unit amplitude and frequency 0.3 Hz shows a sinusoidal output of amplitude 0.5 and the same frequency (Figure 9.3a). The same input forcing produces a nonlinear response of the same fundamental frequency and with an amplitude of approximately 0.5. However, the shape of the response is clearly nonsinusoidal but appears more "squarish," since it contains higher frequency components (Figure 9.3c). The difference becomes much more apparent when these responses are viewed in terms of their corresponding *phase-plane* plots. As described further in the next section, signals generated by systems that are governed by second-order differential equations can be completely characterized by plotting the first time-derivative versus the variable in question. In the examples given, dP_{alv}/dt is plotted against P_{alv}. In the linear case, the phase-plane plot of the system response is an ellipse (Figure 9.3b). In the nonlinear case, the phase-plane plot also shows a closed-loop figure, but the structure of the plot is much more irregular than the ellipse (Figure 9.3d).

Another feature that illustrates the dynamic complexity of nonlinear systems is that, under certain conditions, the response to periodic stimulation at a given frequency can change dramatically if the *amplitude* of the stimulus is varied. Again, we illustrate this point with the

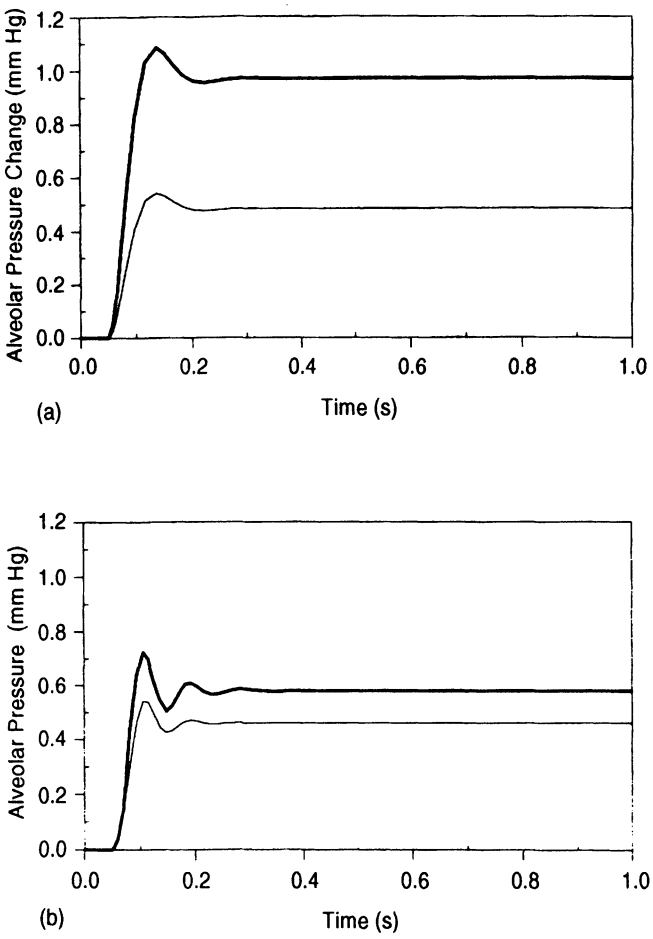

Figure 9.2 (a) Responses of the linear lung mechanics model to a unit step (light tracing) and a step of magnitude 2 in P_{ao}. (b) Responses of the model with nonlinear feedback to the same inputs, showing that the principle of superposition is no longer valid in nonlinear systems.

example of the closed-loop nonlinear lung mechanics model of Figure 9.1b. When the nonlinear model is stimulated by a sinusoidal perturbation in P_{ao} of frequency 0.16 Hz and amplitude 10 mm Hg, the response, as depicted by the time-series and phase-plane plots in the top panel of Figure 9.4, is essentially a very high frequency oscillation that rides on top of the (slower) fundamental frequency. When the forcing amplitude is decreased to 1 mm Hg (middle panel of Figure 9.4), the frequency of the "fast" oscillatory component is decreased and the response contains a mixture of periodic and aperiodic components. Finally, when the forcing amplitude is decreased to less than 0.01 mm Hg (bottom panel of Figure 9.4), the fluctuations in P_{alv} become aperiodic and appear unpredictable. This type of dynamic behavior is known as *deterministic chaos*, since the seemingly random motion is generated by a perfectly deterministic model with no explicit noise input.

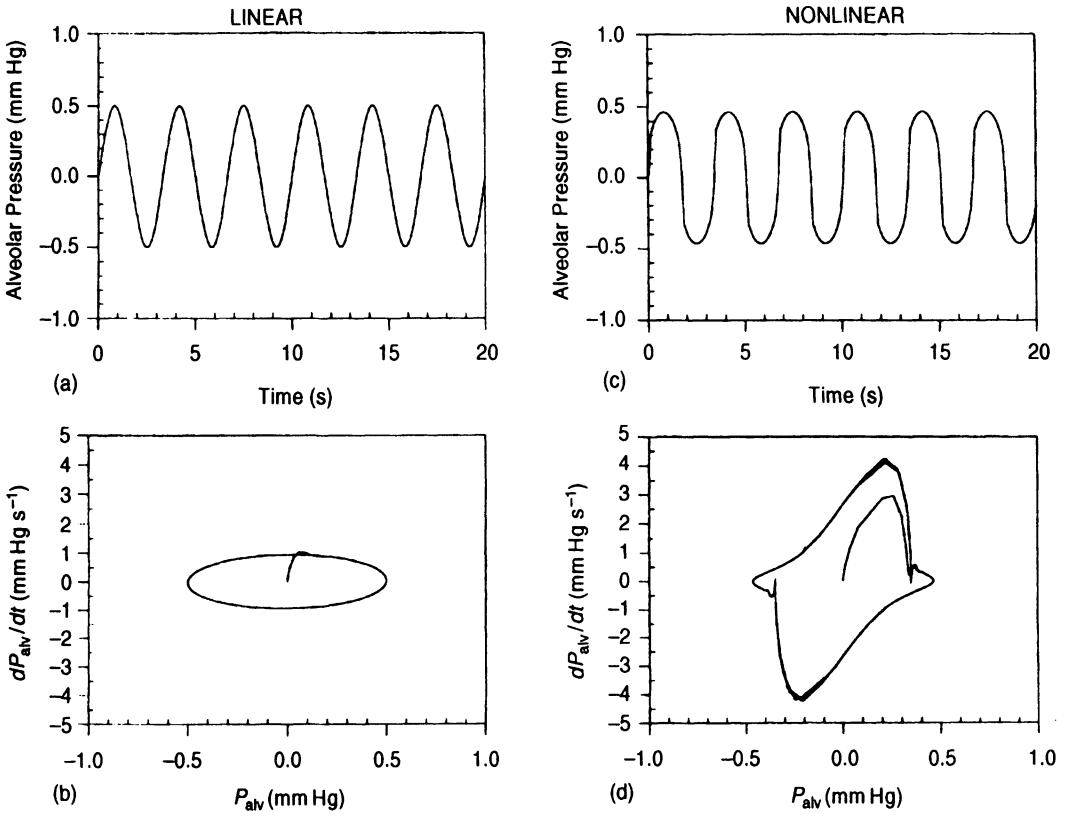

Figure 9.3 Responses of the linear (a) and nonlinear (c) lung mechanics models to sinusoidal forcing in P_{ao}. The corresponding phase-plane plots are displayed in (b) and (d), respectively.

9.2 PHASE-PLANE ANALYSIS

Consider the motion of a simple linear spring–mass system that is characterized by the following second-order differential equation:

$$m\frac{d^2x}{dt^2} + kx = 0 \tag{9.1}$$

The steady-state solution to the above equation is given by:

$$x(t) = A\sin\left(\sqrt{\frac{k}{m}}\,t + \phi\right) \tag{9.2}$$

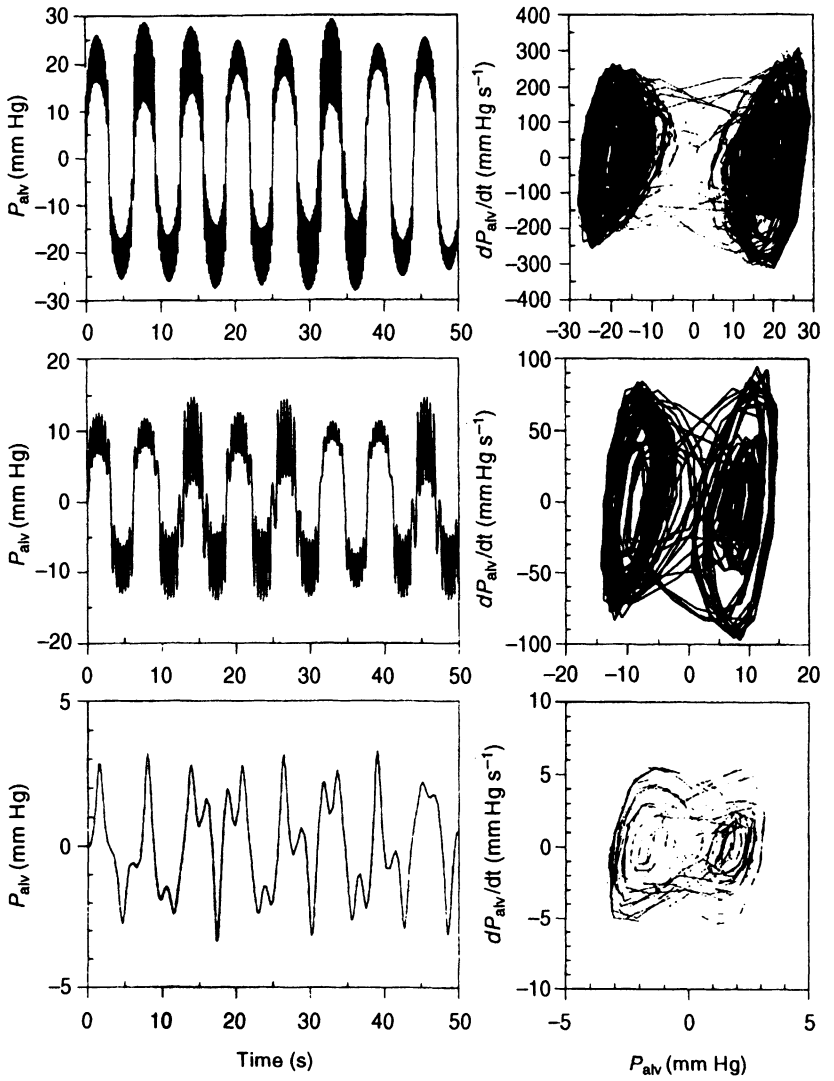

Figure 9.4 Changes in the dynamics of the sinusoidally forced nonlinear lung mechanics model from almost periodic to chaotic as the forcing amplitude is reduced (top to bottom panels). Forcing frequency is 0.16 Hz.

where the constants A and ϕ are determined by the initial conditions, i.e., the initial position and velocity of the mass. If we differentiate Equation (9.2) with respect to time, we obtain the velocity, $y(t)$, of the mass:

$$y(t) = x(t) = \sqrt{\frac{k}{m}} A \cos\left(\sqrt{\frac{k}{m}} t + \phi\right) \tag{9.3}$$

Then, normalizing Equation (9.2) by A and Equation (9.3) by $(k/m)^{1/2}A$, and using the trigonometric equality

$$\sin^2\left(\sqrt{\frac{k}{m}} t + \phi\right) + \cos^2\left(\sqrt{\frac{k}{m}} t + \phi\right) = 1 \tag{9.4}$$

we obtain the following relation between $x(t)$ and $y(t)$:

$$x^2 + \frac{y^2}{k/m} = A^2 \tag{9.5}$$

Equation (9.5) allows the motion of the mass to be completely characterized by a knowledge of the instantaneous position and velocity of the mass, given that the initial position of the mass is also known. As such, x and y represent the *state* of the system. Note that, although x and y are functions of time, Equation (9.5) contains no explicit terms in time. Thus, when y is plotted against x, a "stationary" ellipse appears, similar to that displayed in Figure 9.3b. For different values of A, ellipses of different sizes are generated. Each of these ellipses is known as a *trajectory* of the system, and the plane formed by the position and velocity axes is the *phase plane.*

9.2.1 Local Stability: Singular Points

The above example of a system with second-order dynamics can also be expressed in terms of a set of coupled first-order differential equations involving the position variable, $x(t)$, and the velocity variable, $y(t)$:

$$\frac{dx}{dt} = y \tag{9.6}$$

$$\frac{dy}{dt} = -\frac{k}{m}x \tag{9.7}$$

On the phase plane, the locus of points in which dx/dt (velocity) or dy/dt (acceleration) becomes zero is known as a *nullcline.* In general, the locus of points in the phase plane through which phase trajectories pass with constant slope is termed an *isocline.* The x-nullcline ($dx/dt = 0$) is a special case of an isocline that has infinite slope, while the y-nullcline ($dy/dt = 0$) is an isocline that has zero slope. In the linear oscillator, the x-nullcline coincides with the x-axis of the phase plane, while the y-nullcline lies on the y-axis. At the point where both nullclines intersect (i.e., at the origin), dx/dt and dy/dt are both simultaneously zero. This corresponds to an *equilibrium point,* a point at which there is no motion. Equations (9.6) and (9.7) can also be represented in the form of the following differential equation, in which there is no longer any explicit dependence on time:

$$\frac{dy}{dx} = \frac{-\frac{k}{m}x}{y} \tag{9.8}$$

At the equilibrium point, the numerator and denominator on the right-hand side of Equation (9.8) each becomes zero. As such, equilibrium points are also referred to as *singular points* in phase-plane terminology. Although there is "no motion" at the singular points, they do not necessarily represent stable points of equilibrium. The type of stability in the vicinity of each singular point can yield useful information about overall system dynamics.

Consider a second-order system that can be characterized by the following phase-plane equations (in which $y = dx/dt$):

$$\frac{dx}{dt} = F(x, y) \tag{9.9}$$

$$\frac{dy}{dt} = G(x, y) \tag{9.10}$$

where F and G can be nonlinear functions of x and y. Suppose one of the singular points is at (x_0, y_0). Consider the dynamics of motion at a point (x, y) located in the proximity of the singular point, where

$$x = x_0 + u \tag{9.11}$$

$$y = y_0 + v \tag{9.12}$$

If we use Equations (9.11) and (9.12) to substitute for x and y, respectively, in Equations (9.9) and (9.10) and perform a Taylor expansion about (x_0, y_0), we obtain, after ignoring terms higher than first order, the following expressions for the local dynamics around (x_0, y_0):

$$\frac{du}{dt} = F_x u + F_y v = \frac{\partial F}{\partial x} u + \frac{\partial F}{\partial y} v \tag{9.13}$$

$$\frac{dv}{dt} = G_x u + G_y v = \frac{\partial G}{\partial x} u + \frac{\partial G}{\partial y} v \tag{9.14}$$

where the partial derivative terms (F_x, F_y, G_x, G_y) are all evaluated at the singular point (x_0, y_0). Equations (9.13) and (9.14) can be combined in order to eliminate v, resulting in the following linear second-order differential equation:

$$\frac{d^2u}{dt^2} - (F_x + G_y)\frac{du}{dt} + (F_x G_y - G_x F_y)u = 0 \tag{9.15}$$

The solution to Equation (9.15) is given by

$$u = A_1 e^{\alpha_1 t} + A_2 e^{\alpha_2 t} \tag{9.16}$$

where the constants A_1 and A_2 depend on the initial conditions, and α_1 and α_2 are given by the roots of the following quadratic equation:

$$\alpha^2 - (F_x + G_y)\alpha + (F_x G_y - G_x F_y) = 0 \tag{9.17}$$

The solution for v takes a form similar to that of Equation (9.16), except that the coefficient of each exponential term will be different from the corresponding term in Equation (9.16).

From Equation (9.16), it can be seen that the singular point in question will be *stable* only if the real parts of α_1 and α_2 are both *negative*. For this to be the case, two conditions must hold:

(A) The sum of the roots must be negative, i.e.,

$$F_x + G_y < 0 \tag{9.18}$$

(B) The product of the roots must be positive, i.e.,

$$F_x G_y - G_x F_y > 0 \tag{9.19}$$

Even if the singular point is stable, there is the additional question of whether the associated dynamics is oscillatory. For nonoscillatory dynamics, both roots must be real (i.e., have no imaginary parts):

$$\text{(C)} \qquad (F_x + G_y)^2 - 4(F_x G_y - G_x F_y) > 0 \tag{9.20}$$

Thus, depending on the values of the roots of Equation (9.17), one can have singular points with a variety of dynamics:

1. *Both roots real and negative*: Here, conditions (A), (B), and (C) are all satisfied. This singular point represents a *stable node*: the decay towards this equilibrium point is nonoscillatory.
2. *Both roots complex with negative real parts*: Conditions (A) and (B) are satisfied but not condition (C). The equilibrium point is stable but the decay towards it is oscillatory. This kind of singularity is known as a *stable focus*.
3. *Both roots real and positive*: Here, conditions (B) and (C) are satisfied but not condition (A). This produces an *unstable node*: any infinitesimal perturbation will cause the state point to move away from the singularity but the motion will not be oscillatory.
4. *Both roots complex with positive real parts*: Only condition (B) is satisfied. This produces an *unstable focus*: any infinitesimal perturbation will cause the state point to move away from the singularity with oscillatory dynamics.
5. *Both roots imaginary (zero real parts)*: Since the roots must be conjugate, their sum in this case is zero but their product is a positive real value. Thus, only condition (B) is satisfied. This leads to a *center*, which is considered neutrally stable. The singular point associated with the linear spring–mass system in Equation (9.1) is an example of a center.
6. *Both roots real, one positive and one negative*: Here, condition (C) is satisfied but not condition (B). However, condition (A) may or may not hold, depending on the magnitude of the negative root relative to that of the positive root. This gives rise to a peculiar type of unstable equilibrium point known as a *saddle point*.

9.2.2 Method of Isoclines

While the complete phase portrait of any given second-order system can be arrived at by simply solving the set of coupled first-order differential equations (Equations (9.9) and (9.10)), a good understanding of the dynamics of the system can often be obtained by applying an approximate, semigraphical analysis known as the *method of isoclines*. We illustrate the application of this method here by considering the dynamics of a simple nonlinear system: the pendulum. We assume that this pendulum consists of a heavy steel disk linked by a weightless rigid rod to a vertical fixture (Figure 9.5). If we apply Newton's Second Law to the motion of the bob in the direction tangential to the rod, we obtain the following second-order differential equation:

$$mL \frac{d^2\theta}{dt^2} = -mg \sin\theta \tag{9.21a}$$

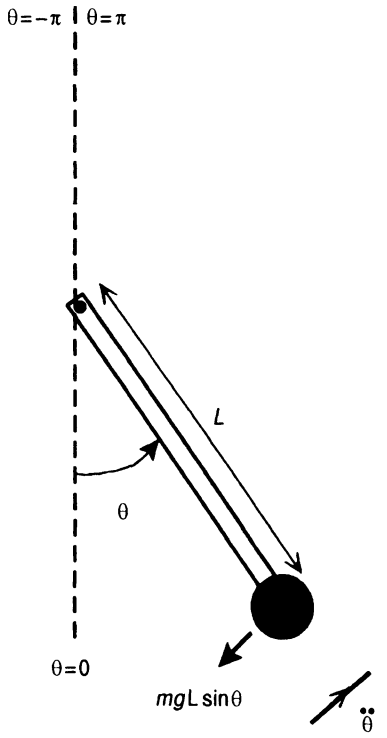

Figure 9.5 Idealized rigid pendulum, showing tangential acceleration and tangential component of gravitational force.

where θ, the angular displacement of the pendulum, is as shown in Figure 9.5. The above equation simplifies to

$$\frac{d^2\theta}{dt^2} + K \sin\theta = 0 \tag{9.21b}$$

where $K\ (= g/L)$ is a constant.

To apply the method of isoclines, we express Equation (9.21b) in the form of the equivalent phase-plane equations. Thus, we have

$$\frac{d\theta}{dt} = \varphi \tag{9.22}$$

$$\frac{d\varphi}{dt} = -K \sin\theta \tag{9.23}$$

These can also be combined to give

$$\frac{d\varphi}{d\theta} = \frac{-K \sin\theta}{\varphi} \tag{9.24}$$

The θ-nullcline (i.e., points along which $d\theta/dt = 0$) is defined by the line $\varphi = 0$, which corresponds to the θ-axis. The φ-nullcline (i.e., along which $d\varphi/dt = 0$) is given by $\sin\theta = 0$. Since θ can take on values between $-\pi$ and π radians, there are three possible solutions for $\sin\theta = 0$ in this range and therefore three φ-nullclines: $\theta = 0$, $\theta = -\pi$ and $\theta = \pi$. However, it should be noted that $\theta = -\pi$ and $\theta = \pi$ correspond to the same physical configuration for the pendulum, i.e., when the bob is vertically above the hinge (see Figure 9.5). Intersection of the θ-nullcline with the three φ-nullclines yields three singular points.

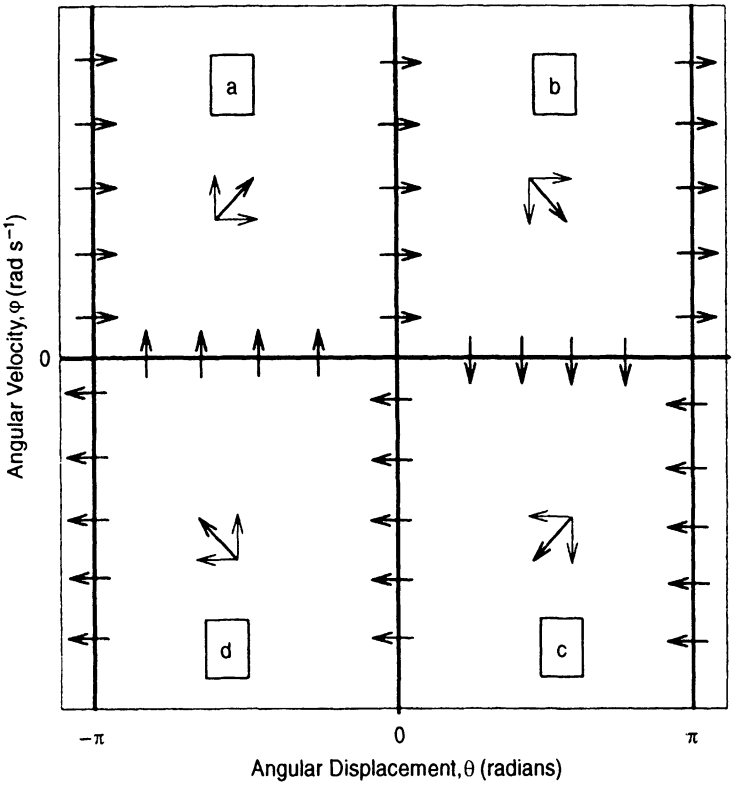

Figure 9.6 Illustration of the method of isoclines. Bold lines represent the nullclines of the system. Arrows indicate the direction of the phase-plane trajectories. a, b, c, and d represent four regions of the phase space in which the general flow directions are different.

Treating θ as the horizontal axis and φ as the vertical axis, these singular points are located at coordinates (0, 0), $(-\pi, 0)$ and $(\pi, 0)$, as indicated by the filled circles in Figure 9.7. The θ- and φ-nullclines also divide up the phase-plane into four regions, labelled a, b, c and d in Figure 9.6. In region a, θ is negative and φ is positive, so that by Equations (9.22) and (9.23), $d\theta/dt > 0$ and $d\varphi/dt > 0$; thus, the trajectories in this region will generally be directed upward and to the right. In region b, both θ and φ are positive, so that from Equations (9.22) and (9.23), $d\theta/dt > 0$ and $d\varphi/dt < 0$; therefore, the flow is now directed downward and to the right. In region c, θ is positive and φ is negative so that $d\theta/dt < 0$ and $d\varphi/dt < 0$. Finally, using similar considerations, it may be shown that in region d, the flow is directed upward and to the left. In Figure 9.6, we have also included arrows to indicate the directions of the flows on the nullclines. Thus, the overall "picture" we obtain from this approximate analysis is that for $\varphi > 0$, the trajectories generally flow from left to right, while for $\varphi < 0$, they flow from right to left. Furthermore, there is also a tendency for the flow to rotate in a clockwise manner around the origin.

Figure 9.7 shows a set of phase trajectories for the pendulum system, computed by solving Equation (9.21b) numerically for $K = 39.5$. Each phase trajectory is obtained by assigning different values to the initial conditions for θ and φ before computing the numerical

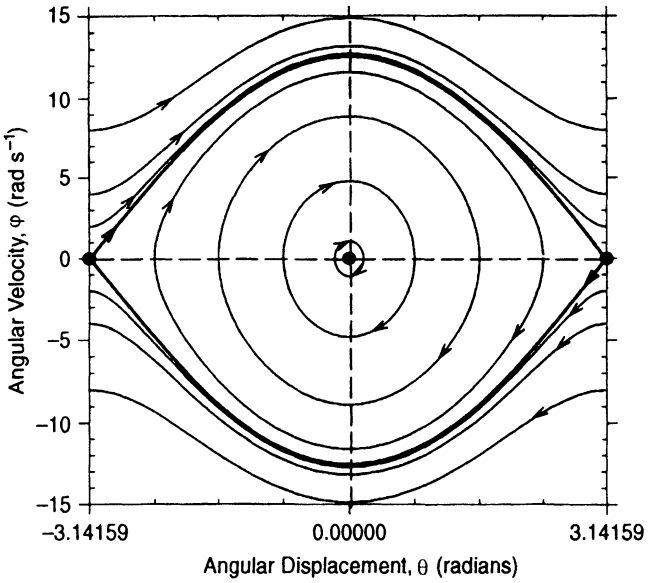

Figure 9.7 Phase-plane portrait of the dynamics of the rigid pendulum. Filled circles represent the singular points, while the bold trajectories represent the separatrices that divide the oscillatory mode (inside) of the pendulum from the rotating mode (outside).

solution. It is clear that the trajectories shown here are consistent with the inferences made using the method of isoclines. For small starting values of θ and φ, the motion of the pendulum is a sinusoidal function of time, oscillating about $\theta = 0$ radians. Applying Equations (9.18), (9.19), and (9.20) to this example, we find that the singular point (0,0) corresponds to a center (imaginary roots). As the starting value for θ approaches $-\pi$ or π, the oscillations become less sinusoidal in character. Finally, if the initial condition for θ is set equal to $-\pi$ or π, the pendulum in principle would achieve an equilibrium position with its bob directly above its hinge. Theoretically, one can imagine that a virtually imperceptible nudge in either direction would send the pendulum swinging in that direction, making a 2π rotation until it comes to rest again with its bob balanced directly above its hinge. Thus, the singular points $(-\pi, 0)$ and $(\pi, 0)$ correspond to saddle points that are attracting when the phase trajectories approach them from one direction but repelling for trajectories in the orthogonal direction. Application of Equations (9.18), (9.19), and (9.20) will allow a verification that $(-\pi, 0)$ and $(\pi, 0)$ are saddle points.

For phase trajectories that begin at $\theta = -\pi$ or $\theta = \pi$ with nonzero velocity (i.e., $\varphi \neq 0$), φ remains uniformly positive or negative over the whole range of θ values. This implies that the motion of the pendulum now is no longer oscillatory, but instead the pendulum simply rotates either in clockwise or anticlockwise manner around its hinge. In Figure 9.7, it is clear that the phase trajectories that lead into or away from the singular points $(-\pi, 0)$ and $(\pi, 0)$ define the boundaries that separate the oscillatory type of motion from the rotational type of motion. These trajectories, which divide the phase plane into regions of differing dynamic modes, are known as *separatrices*.

9.3 NONLINEAR OSCILLATORS

9.3.1 Limit Cycles

The only type of singularity associated with periodic oscillations that was discussed in the previous section is the *center*. The motion associated with a center takes the form of phase trajectories that close on themselves and enclose the singularity. Which particular phase trajectory is taken depends on the initial conditions that preceded the dynamics. For example, in the case of the rigid pendulum, applying an impulsive disturbance to the bob at the end of its swing can increase or decrease the swing amplitude, depending on the relative direction of the disturbance. On the phase portrait, this corresponds to a sudden change in phase trajectory to another of the concentric elliptical (or circular) orbits that enclose the center singularity. In Figure 9.8a, the pendulum bob is given a knock directed towards the equilibrium point ($\theta = 0$) at the end of its swing. This allows it to pass the $\theta = 0$ position with increased velocity, and consequently allows it to achieve an oscillation of larger amplitude. In the phase-plane diagram; this is represented by a change in trajectory from a to b (Figure 9.8a). Since no damping is present, the state-point will not return to the original phase trajectory unless another externally imposed disturbance forces it to do so.

Many physiological oscillators exhibit a behavior that is quite different from that displayed in Figure 9.8a. On the phase plane, these oscillations assume the form of a stable, closed trajectory called a *limit cycle*. What distinguishes the limit cycle from the type of oscillation discussed previously is that, although external perturbations can move the state point away from the limit cycle trajectory, it eventually always rejoins the original trajectory. This is illustrated in Figure 9.8b. Whether the state point is moved to a location outside the limit cycle (point a in Figure 9.8b) or a location inside the limit cycle (point b in Figure 9.8b), the original oscillatory behavior is always reestablished after some time.

9.3.2 The van der Pol Oscillator

In 1928, van der Pol and van der Mark proposed the first dynamic model of oscillatory activity in the heart. Their model consisted of the following second-order nonlinear differential equation:

$$\frac{d^2x}{dt^2} - c(1 - x^2)\frac{dx}{dt} + x = 0 \tag{9.25}$$

where the constant $c > 0$. The phase-plane properties of the van der Pol equation are most conveniently explored by applying *Lienard's transformation*, i.e.,

$$y = \frac{1}{c}\frac{dx}{dt} + \frac{x^3}{3} - x \tag{9.26a}$$

Differentiating Equation (9.26a) with respect to time, and substituting the result into Equation (9.25), we obtain

$$\frac{dy}{dt} = -\frac{x}{c} \tag{9.27}$$

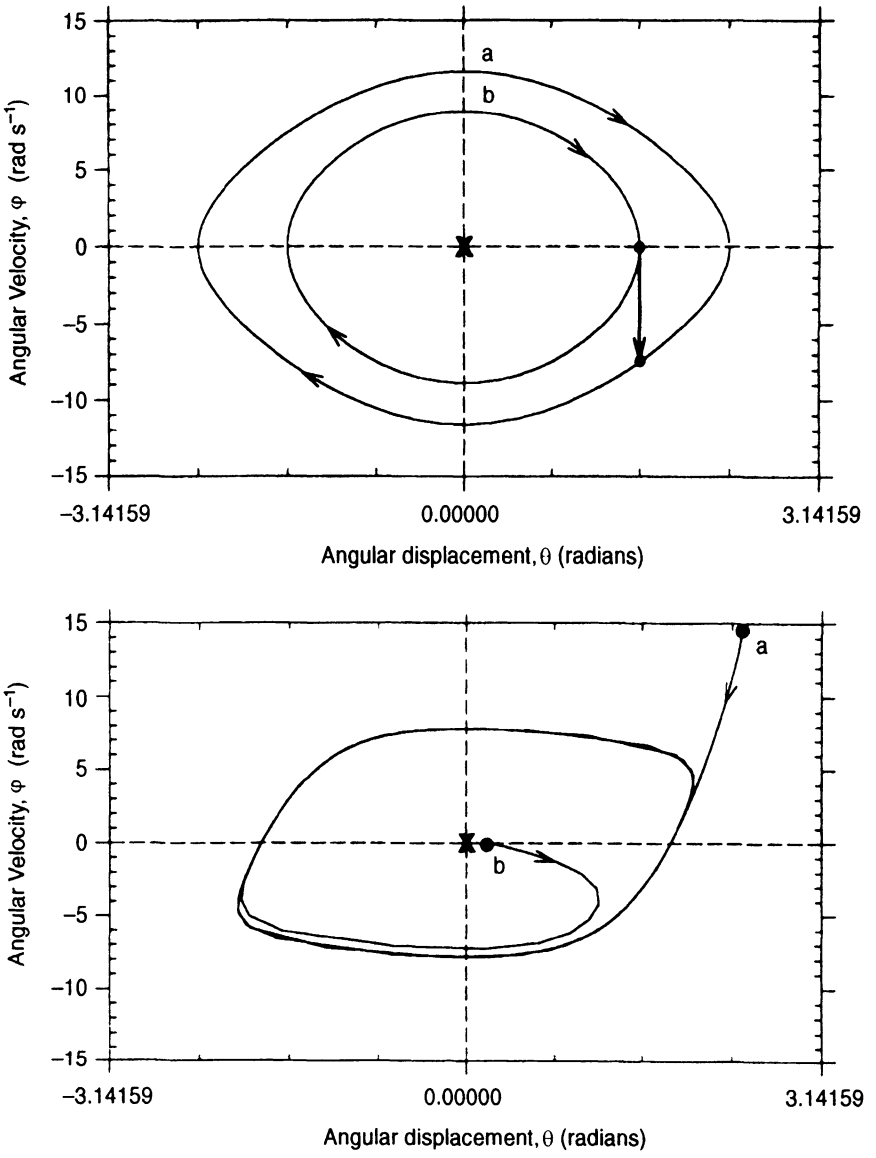

Figure 9.8 Differences between a non-limit-cycle oscillator (a) and a limit-cycle oscillator (b). In the former, external disturbance (bold arrow) moves the phase trajectory to a different orbit (b vs. a) around the center. In the stable limit cycle, the state point always returns to its original trajectory even after an external disturbance moves it to a different location.

Rearranging Equation (9.26a), we have:

$$\frac{dx}{dt} = c\left(y - \frac{x^3}{3} + x\right) \tag{9.26b}$$

Equations (9.26b) and (9.27) form a set of coupled first-order differential equations which do not have a closed-form analytic solution. However, the techniques of Section 9.2 can be employed to provide a rough picture of the phase portrait of this dynamic system.

First, we deduce the phase-plane locations of the nullclines. The x-nullcline ($dx/dt = 0$) corresponds to the locus defined by the cubic function:

$$y = \frac{x^3}{3} - x \tag{9.28}$$

The y-nullcline ($dy/dt = 0$) is given by the vertical axis, or

$$x = 0 \tag{9.29}$$

The x- and y-nullclines intersect at only one point, i.e., at the origin (0, 0). We determine the nature of the singular point found at (0,0) by evaluating the coefficients of Equation (9.17) and subsequently the roots of the characteristic equation. Assuming that

$$F(x, y) = c\left(y - \frac{x^3}{3} + x\right) \tag{9.30}$$

and that

$$G(x, y) = -\frac{x}{c} \tag{9.31}$$

the characteristic equation describing the dynamics in the vicinity of (0, 0) takes the form:

$$\alpha^2 - c\alpha + 1 = 0 \tag{9.32}$$

Thus, condition (A) is clearly not satisfied while condition (B) is valid for all values of c. Whether condition (C) is satisfied depends on the value of c. When $c \geq 2$, the roots of Equation (9.32) will be real and positive, in which case, the singular point will be an unstable node. However, when $c < 2$, the roots become complex with positive real parts; in this case, the singular point is an unstable focus. Therefore, for all feasible values of c, the equilibrium point at the origin will be an unstable one.

The nullclines divide the phase plane into four major regions, as shown in Figure 9.9. In region a, $x > 0$ and $y > x^3/3 - x$. Therefore, from Equation (9.26b), $dx/dt > 0$ and from Equation (9.27), $dy/dt < 0$. This means that the phase trajectories here in general would be directed downward and to the right. In region b, $x > 0$ and $y < x^3/3 - x$, so that $dx/dt < 0$ and $dy/dt < 0$, and the phase trajectories would tend to point downward and to the left. Applying similar considerations, the pattern of flow is upward and to the left in region c, and upward and to the right in region d. For consistency, the directions of flow on the nullclines must be as displayed in Figure 9.9. Thus, in general, there is a clockwise flow of phase trajectories around the origin; however, at the same time, because of the unstable node or focus, the trajectories are also directed away from the origin.

To complete the picture, we numerically integrate Equations (9.26b) and (9.27) for given values of c, but with several different initial conditions. This can be achieved quite easily by implementing the system defined by Equations (9.26b) and (9.27) as a SIMULINK model. This model, the source code for which may be found in the SIMULINK file "`vdpmod.mdl`," is displayed in Figure 9.10. Figure 9.11a shows an example of the oscillatory dynamics generated by the van der Pol model for $c = 3$. This saw-toothed type of waveform is commonly referred to as a *relaxation oscillation*. A more complete representation of van der Pol dynamics is displayed in Figure 9.11b, which shows the

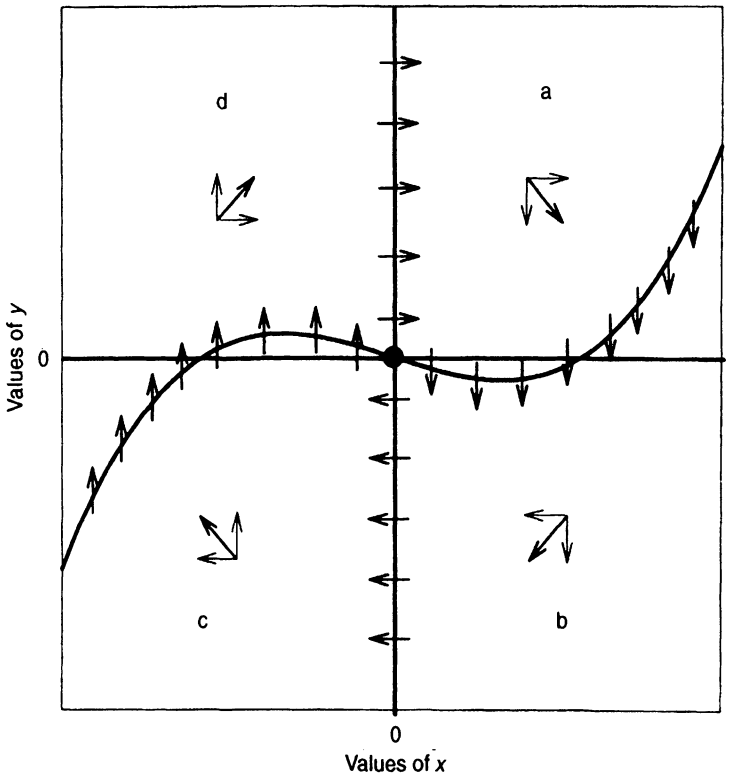

Figure 9.9 Method of isoclines applied to the van der Pol model. Arrows indicate direction of phase-plane trajectories. a, b, c, and d represent four regions in which the general flow directions are different. The nullclines ($y = x^3/3 - x$ and $x = 0$) are shown as bold lines. The filled circle at the origin represents the only singular point for this system.

portraits for six phase trajectories that originate from different starting points (or initial conditions, shown as filled circles) in the phase space. The x-nullcline (shown as the dotted curve) is displayed for reference. Note that phase trajectories that originate from inside the limit cycle move away from the singular point toward the limit cycle, whereas the phase trajectories from outside the limit cycle move inward toward the limit cycle. All trajectories tend to circulate around the origin in a clockwise pattern, as predicted in Figure 9.9.

One feature that distinguishes a nonlinear oscillator, such as the van der Pol system, from a linear oscillatory system is that the former can exhibit the phenomenon of *entrainment* or *phase-locking*. The coupling of two linear systems with different natural oscillatory frequencies leads to *beating*, in which the combined output shows the original two frequencies of oscillation plus a new oscillation that corresponds to the difference between the two frequencies. However, when a nonlinear oscillator is driven by an external periodic stimulus whose frequency is quite different from the former, the output of the oscillatory system will contain a mixture of components that result from the interaction of the driving periodicity and the natural oscillation. As the driving frequency approaches the natural frequency of the nonlinear oscillator, there will be a range of frequencies over which the

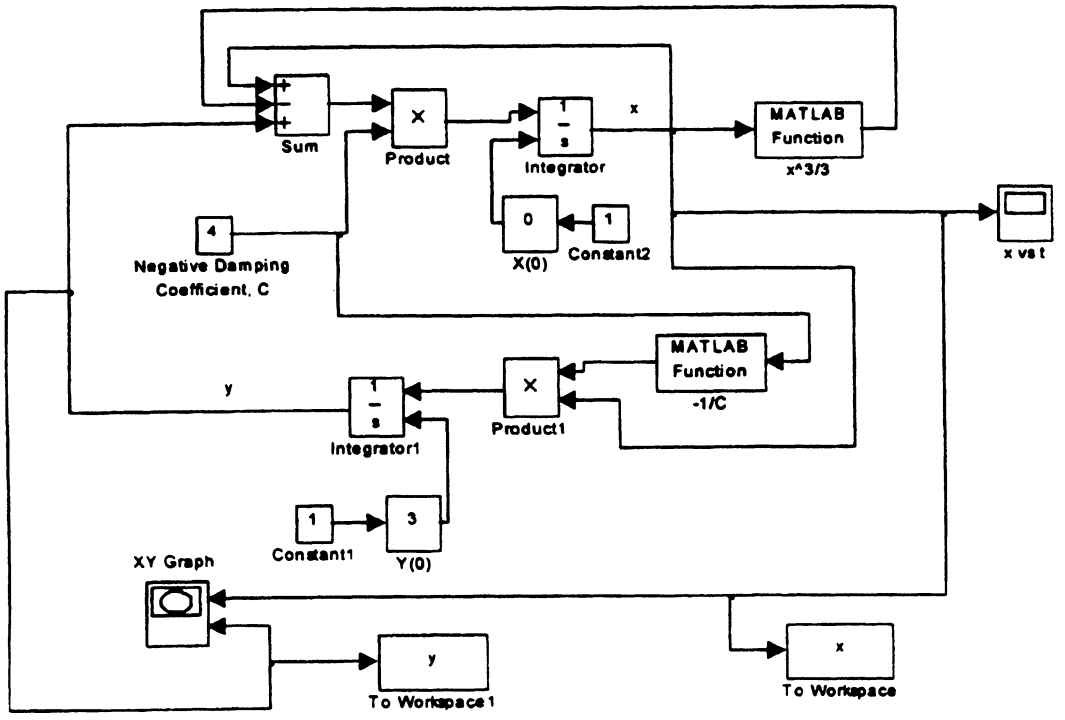

Figure 9.10 SIMULINK implementation of the van der Pol oscillator. This model is contained in SIMULINK model file "`vdpmod.mdl`."

nonlinear system will adopt the frequency of the driving stimulus. This is illustrated for the case of the van der Pol oscillator in Figure 9.12. Here, the system of equations becomes

$$\frac{dx}{dt} = c\left(y - \frac{x^3}{3} + x\right) \tag{9.33}$$

and

$$\frac{dy}{dt} = -\frac{x}{c} + \frac{B}{c}\sin 2\pi ft \tag{9.34}$$

where B and f represent the amplitude and frequency, respectively, of the periodic stimulus. As shown in Figure 9.12a, the natural frequency of the van der Pol oscillator is 0.113 Hz. When this system is stimulated periodically at frequencies that are substantially lower (e.g., Figure 9.12b) or higher (e.g., Figure 9.12e) than 0.113 Hz, the result is a mixture of the forcing and natural frequencies. However, at frequencies close to 0.113 Hz, the van der Pol system adopts the frequencies of the driving stimulus (Figures 9.12c and 9.12d). Frequency entrainment is an important phenomenon from a practical standpoint, since it forms the basis on which heart pacemakers work. Frequency entrainment also explains the synchronization of many biological rhythms to the light–dark cycle, the coupling between respiration and blood pressure, as well as the synchronization of central pattern generators during walking and running.

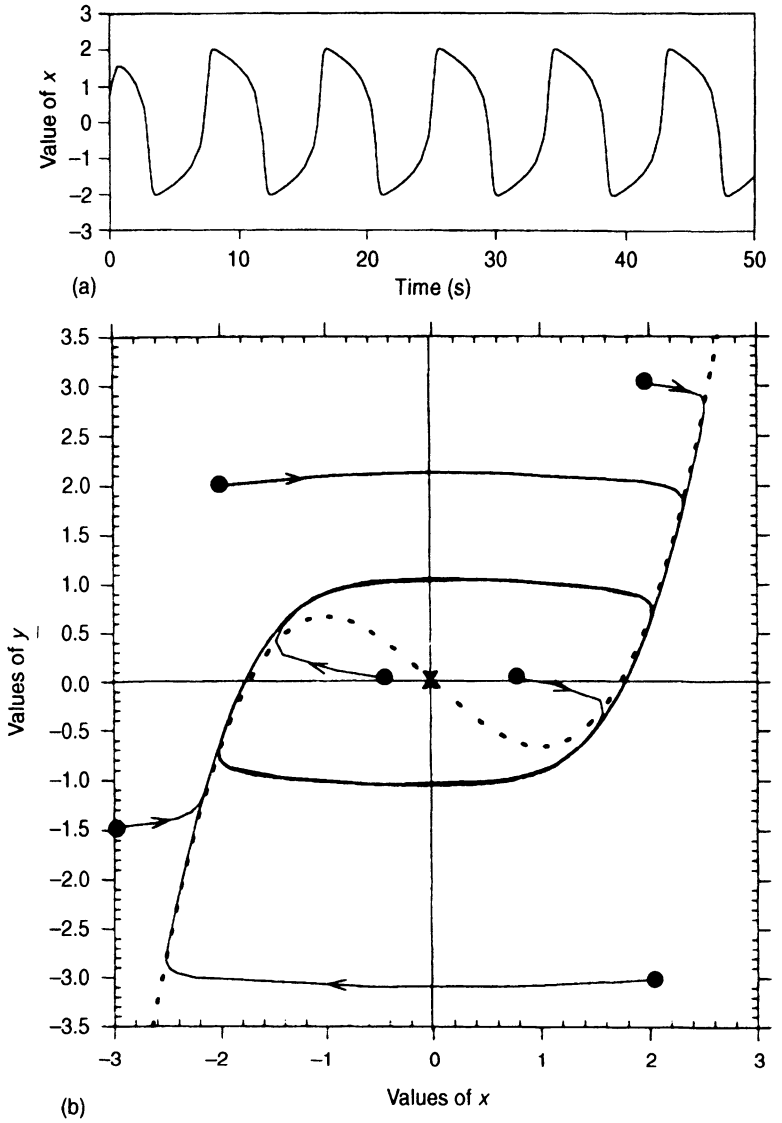

Figure 9.11 (a) Time-course of oscillatory activity generated by the van der Pol model. (b) Phase portrait showing limit cycle formed by several trajectories initiated at different starting points (shown as filled circles). The x-nullcline is shown as the dotted curve, while the singular point at the origin is marked as a cross. Note consistency of flows with Figure 9.9.

9.3.3 Modeling Cardiac Dysrhythmias

Under normal circumstances, the cardiac cycle originates as electrical activity generated by the sinoatrial node. This impulse spreads through the atrial musculature, the atrioventricular node and finally through the Purkinje network of conducting fibers to elicit ventricular contraction. A common class of disorders, known as *atrioventricular heart block*, can occur in which the relative timing between atrial and ventricular contractions becomes impaired.

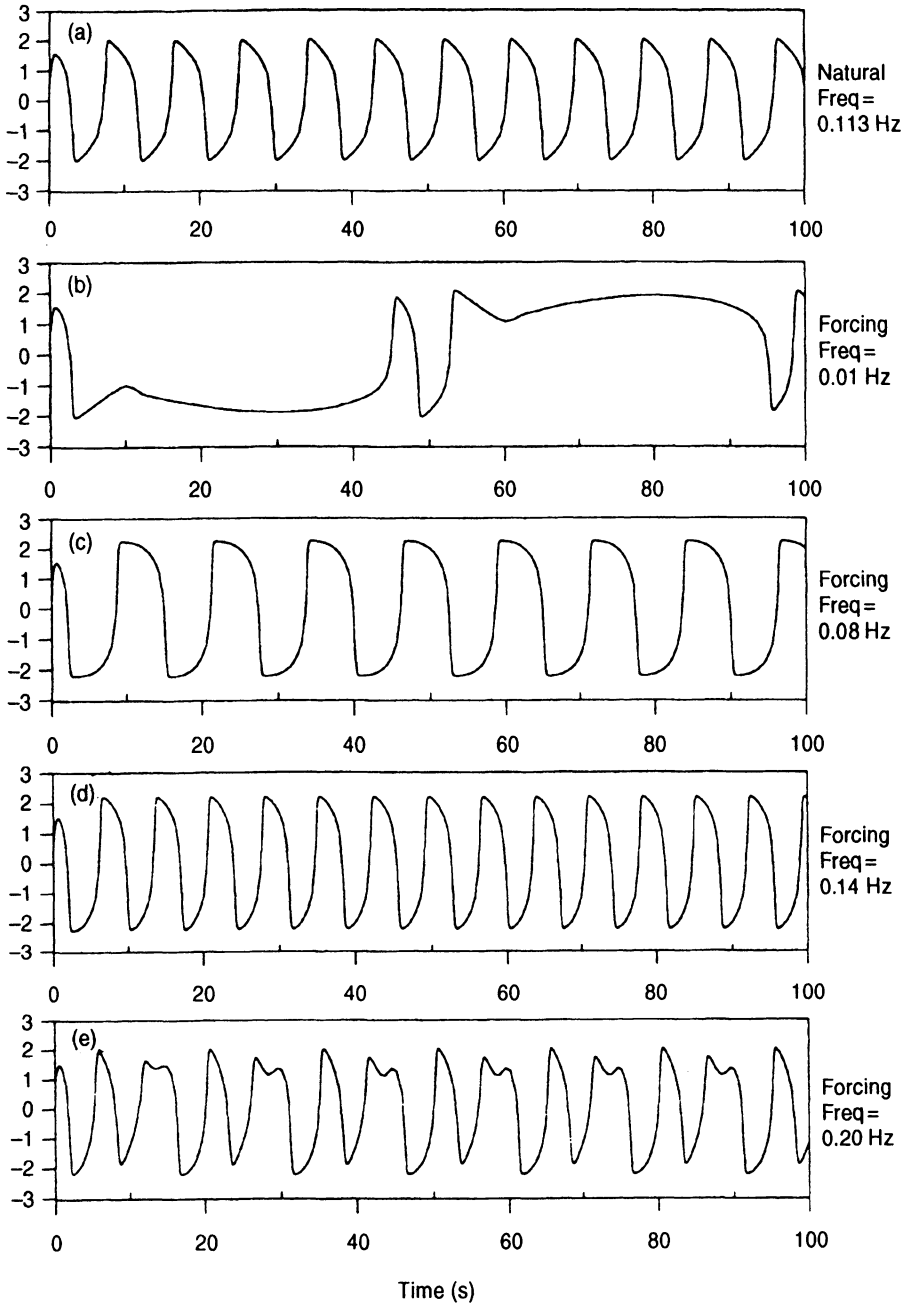

Figure 9.12 Responses of the van der Pol oscillator to external sinusoidal forcing. The top panel (a) shows spontaneous oscillations at 0.113 Hz. The system becomes entrained to the frequency of the external forcing when the latter is close to the natural frequency of the oscillator.

One line of thought postulates that these dysrhythmias are the result of dynamic interaction among two or more coupled nonlinear oscillators in heart tissue. One of the simplest oscillator models that can demonstrate this type of phenomena is the *Poincaré oscillator.* This dynamic system is characterized by the following set of differential equations:

$$\frac{dr}{dt} = ar(1 - r) \tag{9.35}$$

and

$$\frac{d\Phi}{dt} = 2\pi \tag{9.36}$$

where r represents the radial coordinate and $\Phi(-\infty < \Phi < \infty)$ represents the angular coordinate (in radians) of the state point in the phase plane. These dynamics give rise to a limit cycle that rotates anticlockwise on the unit circle (Figure 9.13). As such, it is more convenient to define the new angular coordinate, ϕ, as follows:

$$\phi = \frac{\Phi}{2\pi} (\text{mod } 1) \tag{9.37}$$

so that $0 \leq \phi < 1$. ϕ is also known as the (normalized) *phase* of the oscillation.

Guevara and Glass (1982) considered what would occur if this oscillator were perturbed by an isolated, brief stimulus in the limit where $a \to \infty$. This is illustrated in Figure 9.13. The stimulus is represented by the heavy arrow that shifts the state point from its prestimulus location, corresponding to phase ϕ (shown in black), to its poststimulus location, corresponding to phase θ (shown in grey). The length of the arrow represents b, the magnitude of the stimulus. Because a is infinite, the new state point moves instantaneously along the radial direction back to the limit cycle. It can be seen that when $0 < \phi < 0.5$, the state point is pushed back to a location that it had previously traversed; thus, the perturbation causes a *phase delay.* On the other hand, when $0.5 < \phi < 1$, the same stimulus would push the state point to a location further along the limit cycle; in this case, the perturbation causes a *phase advance.* This type of phenomenon is known as *phase resetting.* By careful consideration of

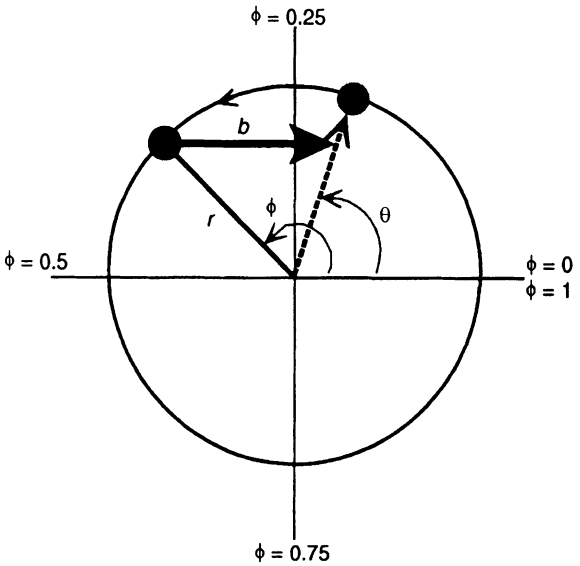

Figure 9.13 The Poincaré oscillator. Application of a brief stimulus of magnitude b leads to a resetting of the phase from ϕ to θ (old state point shown as black circle, new state point shown as grey circle). When $0 < \phi < 0.5$, the perturbation produces a delay in phase, but when $0.5 < \phi < 1$, the same stimulus causes an advance in phase.

the geometrical details of Figure 9.13, it can be shown that the new phase θ is related to the old phase ϕ through the following relationship:

$$\cos 2\pi\theta = \frac{b + \cos 2\pi\phi}{\sqrt{1 + 2b\cos 2\pi\phi + b^2}} \tag{9.38}$$

However, depending on the magnitude of the stimulus, b, Equation (9.38) can yield very different-looking functions that relate θ to ϕ; these functions are termed *phase transition curves*. As illustrated in Figure 9.14, when $b < 1$ (*weak resetting*), there is a phase delay (i.e., $\theta < \phi$) for the range $0 < \phi < 0.5$ and a phase advance (i.e., $\theta > \phi$) for $0.5 < \phi < 1$, as noted earlier. Since the average slope of the phase transition curve is unity, this type of phase resetting is also commonly referred to as *type 1* resetting. However, when $b > 1$ (*strong resetting*), the effect of the perturbation on the trajectory of the state point becomes interesting and somewhat surprising at first glance. As ϕ increases from zero toward 0.5, θ initially increases but subsequently decreases so that, when ϕ attains the value of 0.5, θ becomes zero. The reason for this form of relationship may be better understood if one considers what happens for the case when ϕ equals 0.5: the perturbation forces the state point to a location on the horizontal axis that is past the center of the circle. The closest point on the limit cycle to this new state location is at $\phi = 0$. When ϕ increases beyond 0.5, perturbation of the state point leads to a resetting of phase to points that begin at $\phi = 1$, decrease below 1, but eventually increase back toward 1. As a result, the phase transiiton curve shows an apparent discontinuity and the average slope becomes zero (Figure 9.14, bold curve). This kind of resetting is known as *type 0* resetting.

Equation (9.38) characterizes the effect on the Poincaré oscillator of a single, isolated stimulus, delivered when the phase of the oscillation is ϕ. This can be extended to produce a corresponding formula that characterizes how a periodic train of impulses would affect the

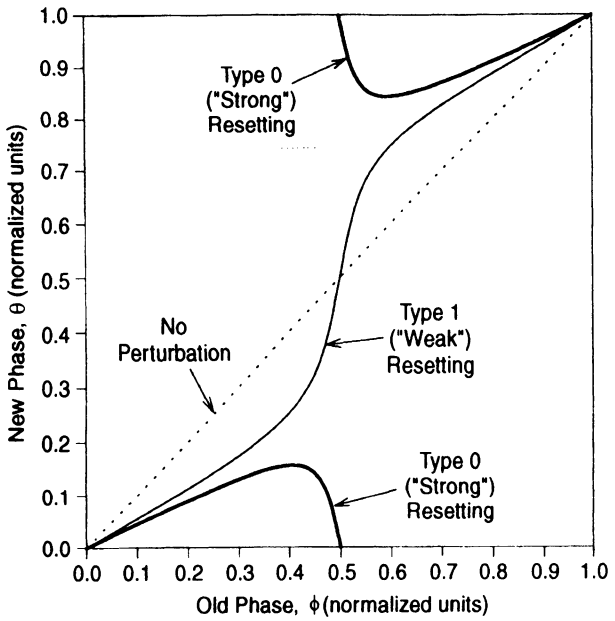

Figure 9.14 Phase transition curves for the Poincaré oscillator. The dotted (identity) line represents the case in which there is no perturbation. When the system is perturbed by a brief stimulus of magnitude b ($b < 1$), type 1 or weak resetting occurs (light solid curve). However, when $b > 1$, type 0 or strong resetting occurs (bold solid curve) in which there is an apparent discontinuity at $\phi = 0.5$.

behavior of the oscillator. If ϕ_i is the phase of the oscillator immediately prior to the ith stimulus, then the phase just before the next stimulus occurs is given by

$$\phi_{i+1} = \frac{1}{2\pi}\cos^{-1}\left(\frac{b + \cos 2\pi\phi_i}{1 + 2b\cos 2\pi\phi_i + b^2}\right) + \frac{T_s}{T_0} \tag{9.39}$$

where T_0 is the period of the limit cycle and T_s is the interval between successive stimuli. Guevara and Glass showed that the nonlinear finite difference equation represented by Equation (9.39) can give rise to dynamics that are qualitatively similar to the dysrhythmias that have been observed in the electrocardiogram. To reproduce their simulations, we have developed the SIMULINK implementation (labeled "`poincare.mdl`") of the Poincaré model, as shown in Figure 9.15. Since the constant a in Equation (9.35) is taken to be infinitely large, the state point is assumed to instantaneously return to the limit cycle after each perturbation by the external stimulus. As such, r is assumed to be always equal to unity, and the radial dynamics in Equation (9.35) are neglected. In this model, we have also assumed that, whenever the rotating arm of the oscillator passes through $\phi = 0$, the system will generate a unit impulse (simulating a neural spike). The "stimulus period" ("`tau`" in Figure

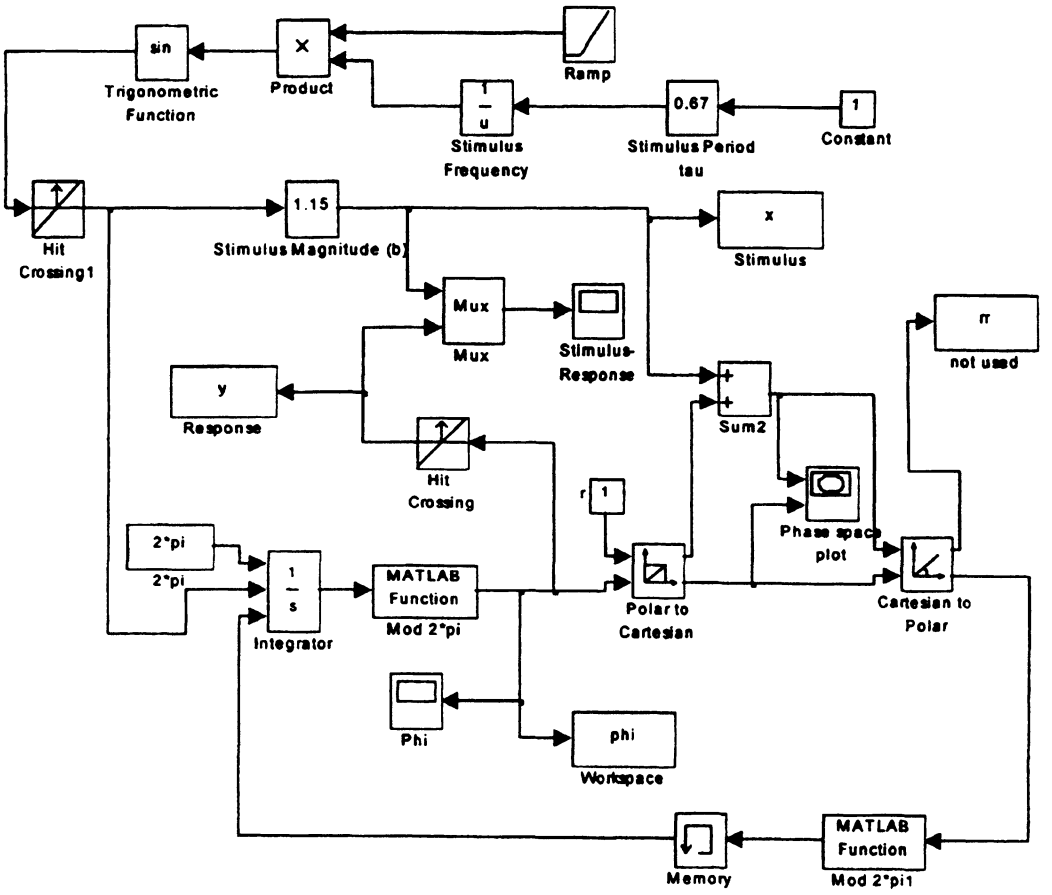

Figure 9.15 SIMULINK implementation of the Poincaré oscillator model. This model may be found in the file "`poincare.mdl`."

9.15) that has to be specified prior to running the simulation is normalized with respect to the natural period of the limit cycle, i.e., `tau` $= T_s/T_0$.

Figure 9.16 displays some examples of the response of the Poincaré oscillator to a periodic stimulation of magnitude $b = 1.13$. In Figure 9.16a, the period of the stimulation is 75% of the length of the natural oscillatory cycle of the model. Entrainment occurs so that the Poincaré oscillator "fires" at approximately the same frequency as the external periodic stimulus. This kind of entrainment is also called *1:1 phase-locking*. When the normalized stimulation period is reduced to 0.69 (Figure 9.16b), the Poincaré oscillator now alternates between a long interspike interval and a short interspike interval. For every two stimulus spikes, the system responds with one long interval and one short interval; then the pattern repeats itself. This type of phenomenon is known as *2:2 phase-locking*. With further decrease of T_s/T_0 to 0.68 (Figure 9.16c), four stimulus spikes give rise to four response impulses, but the time relationship between each stimulus spike and its corresponding response is different for the four pairs, producing *4:4 phase-locking*. In Figure 9.16d, where T_s/T_0 is decreased to 0.65, the periodicity in the response disappears. Now the response spikes appear in an unpredictable fashion, giving rise also to skipped beats (e.g., at $t \sim 2.5$ s and $t \sim 4.5$ s in Figure 9.16d). Guevara and Glass have argued that this pattern reflects chaotic dynamics arising in this highly nonlinear system. Finally, in Figure 9.16e, decreasing T_s/T_0 to 0.6 leads to a reemergence of periodicity in the response. However, under these conditions, four stimulus spikes correspond to only two response spikes, producing what is known as *4:2 phase-locking*.

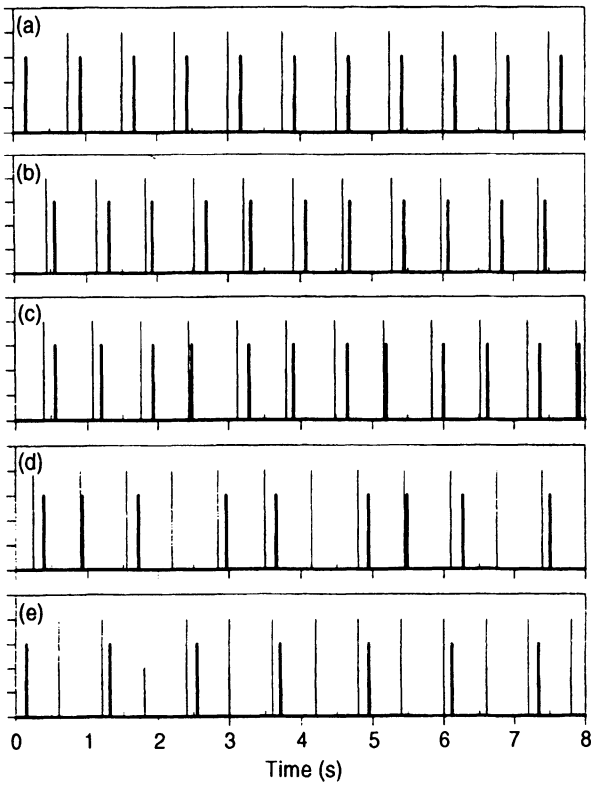

Figure 9.16 Responses (heavy bars) of the Poincaré oscillator to periodic stimulation (light bars) of magnitude $b = 1.13$. The different panels represent responses to different stimulation periods: $T_s/T_0 = 0.85$, 0.69, 0.68, 0.65, and 0.60 in panels (a), (b), (c), (d), and (e), respectively. See text for further details.

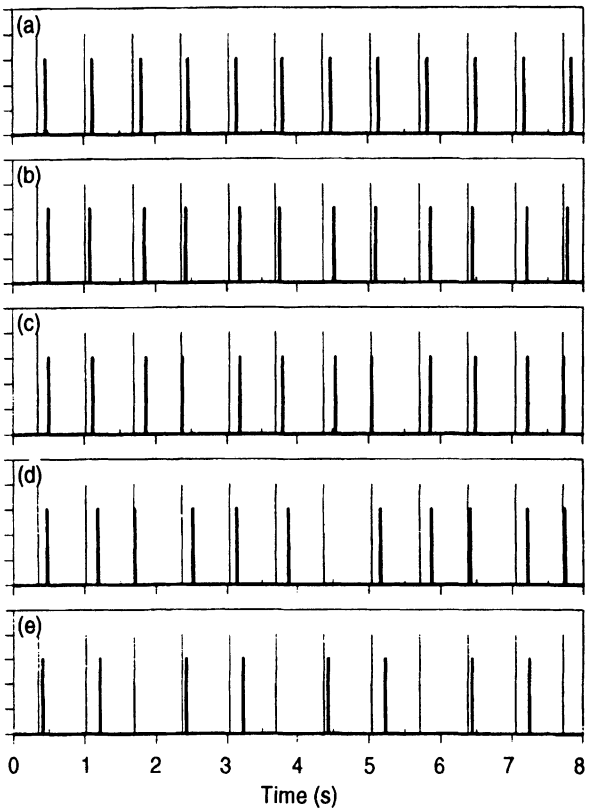

Figure 9.17 Responses (heavy bars) of the Poincaré oscillator to periodic stimulation (light bars) of period $T_s/T_0 = 0.67$. The different panels represent responses to different stimulation magnitudes: $b = 1.40$, 1.22, 1.15, 1.12, and 1.02 in panels (a), (b), (c), (d), and (e), respectively. See text for further details.

The changes in dynamics exhibited by the Poincaré oscillator or any nonlinear system that occur abruptly as a system parameter is decreased or increased are commonly referred to as *bifurcations*. In the examples considered above, the bifurcations occurred at the points where changes in the value of the stimulus period led to sudden changes from one type of phase-locking to another mode. Bifurcations also occur when the magnitude of the stimulus (b) is continually varied. Figure 9.17 shows examples of the model response to periodic stimulation when T_s/T_0 is kept constant at 0.67 but the stimulus magnitude is varied. In Figure 9.17a, when $b = 1.4$, there is 1:1 phase-locking. Decreasing b to 1.22 leads to 2:2 phase-locking (Figure 9.17b), and subsequently, 4:4 phase-locking when $b = 1.15$ (Figure 9.17c). Decreasing b a little further to 1.12 produces chaotic dynamics (Figure 9.17d). Finally, with b decreased to 1.02, the system once again exhibits periodic dynamics (Figure 9.17e). There is now 3:2 phase-locking of the type where the stimulus–response spike interval becomes progressively longer until the Poincaré oscillator misses a beat (e.g., at $t \sim 2$ s and $t \sim 4$ s in Figure 9.17e). This kind of pattern is similar to the clinically observed electrocardiographic phenomenon known as "second-degree AV (atrioventricular node) block with Wenckebach periodicity."

9.4 THE DESCRIBING FUNCTION METHOD

9.4.1 Methodology

The describing function method, sometimes also known as the method of *harmonic balance*, is useful in determining the conditions that produce limit cycles in relatively simple nonlinear systems. It may be viewed as an extension of the Nyquist stability criterion discussed in Chapter 6. The method assumes a closed-loop nonlinear model of the type displayed in Figure 9.18. This system can be decomposed into two parts: a linear portion that contains dynamic features, $G(s)$, and a static nonlinear component, characterized by the function $F(\epsilon)$. It is also assumed that this system is oscillating at some fundamental frequency ω (given in radians per unit time) without any input perturbation (i.e., in Figure 9.18, $u = 0$). In general, the output x of the nonlinear subsystem will be a periodic oscillation with fundamental frequency plus its harmonic components. This can be expressed as a Fourier series:

$$x(t) = X_0 + \sum_{n=1}^{\infty}(a_n \sin n\omega t + b_n \cos n\omega t) \tag{9.40a}$$

On the other hand, if we assume the linear "plant" subsystem to be low-pass in nature, the harmonics in x will be filtered out and the output, y, of the linear subsystem is likely to be approximately sinusoidal in form. Since ϵ is equal to the negative of y in the absence of any external input, we can assume that

$$\epsilon(t) = E \sin \omega t \tag{9.40b}$$

And for purposes of assessing stability of the closed-loop system, we focus only on the fundamental component of $x(t)$, so that from Equation (9.40) we obtain

$$x(t) \approx X_0 + a_1 \sin \omega t + b_1 \cos \omega t \tag{9.41}$$

The *describing function*, *DF*, of the nonlinearity $F(\cdot)$ is defined as the complex coefficient for the fundamental frequency output divided by the input signal amplitude. The mathematical definition is as follows:

$$DF(E) = \frac{a_1 + jb_1}{E} \tag{9.42}$$

In Equation (9.42), *DF* is shown explicitly to be a function of the input amplitude, E. Although, in principle, *DF* can also be a function of frequency, this dependence is rare under

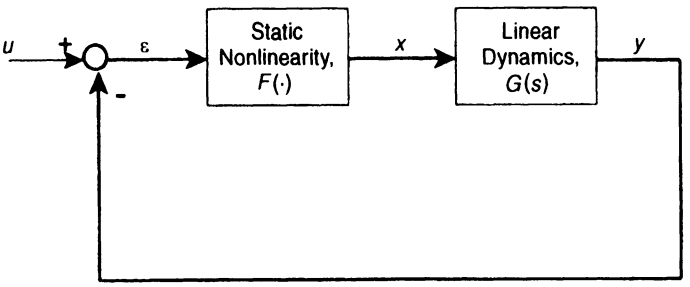

Figure 9.18 Closed-loop nonlinear control system with static nonlinearity and linear dynamic components.

most practical circumstances. In general, the nonlinearity $F(\cdot)$ is assumed to be static, and therefore, independent of frequency.

If we let $\theta = \omega t$, then by making use of the property of orthogonality for $\sin\theta$, we can deduce a_1 by multiplying both sides of Equation (9.41) by $\sin\theta$ and then integrating over the range of 0 to 2π. After simplification and rearrangement of terms, we obtain

$$a_1 = \frac{1}{\pi}\int_0^{2\pi} x(\theta)\sin\theta\, d\theta \tag{9.43}$$

Similarly, it can be shown that

$$b_1 = \frac{1}{\pi}\int_0^{2\pi} x(\theta)\cos\theta\, d\theta \tag{9.44}$$

Since $x(\theta)$ is periodic, changing the range of integration in Equations (9.43) and (9.44) will not alter the values of a_1 and b_1. For reasons that will become self-evident as our discussion proceeds, we choose to change the integral limits in Equation (9.43) and (9.44) to the range $-\pi/2$ to $3\pi/2$. Also, we introduce the following change of variable:

$$z = \sin\theta \tag{9.45}$$

so that the differentials dx and $d\theta$ are related by

$$dz = \cos\theta\, d\theta = \pm\sqrt{1 - z^2}\, d\theta \tag{9.46}$$

Note that the square-root term in Equation (9.46) will take on positive values when $-\pi/2 < \theta < \pi/2$ and negative values when $\pi/2 < \theta < 3\pi/2$. Thus, Equation (9.44) becomes

$$\begin{aligned} b_1 &= \frac{1}{\pi}\left(\int_{-\pi/2}^{\pi/2} x(\theta)\cos\theta\, d\theta + \int_{\pi/2}^{3\pi/2} x(\theta)\cos\theta\, d\theta\right) \\ &= \frac{1}{\pi}\left(\int_{-1}^{1} x(z)\, dz + \int_{1}^{-1} x(z)\, dz\right) = 0 \end{aligned} \tag{9.47}$$

The result derived from Equation (9.47) is important, as it implies that the imaginary part of DF will be negative as long the nonlinear function $F(\cdot)$ is *single-valued*. If there is hysteresis in the nonlinearity, the two integrals in Equation (9.47) (second line) would not be equal in magnitude and opposite in sign, and, as a consequence, b_1 would not be zero.

The same analysis applied to Equation (9.43) yields the following result for a_1:

$$\begin{aligned} a_1 &= \frac{1}{\pi}\left(\int_{-\pi/2}^{\pi/2} x(\theta)\sin\theta\, d\theta + \int_{\pi/2}^{3\pi/2} x(\theta)\sin\theta\, d\theta\right) \\ &= \frac{1}{\pi}\left(\int_{-1}^{1} x(z)\frac{z}{\sqrt{1-x^2}}\, dz + \int_{1}^{-1} x(z)\frac{-z}{\sqrt{1-z^2}}\, dz\right) \\ &= \frac{2}{\pi}\int_{-1}^{1} x(z)\frac{z}{\sqrt{1-z^2}}\, dz \end{aligned} \tag{9.48}$$

The following expression, analogous to the Nyquist stability criterion, provides the conditions under which a limit cycle of amplitude E and angular frequency ω might exist:

$$1 + DF(E)G(j\omega) = 0 \tag{9.49a}$$

Note the similarity in form between the above equation and Equation (6.8), which characterizes the condition in which any *linear* closed-loop system becomes unstable. One

might consider Equation (9.49a) to be an extension of the Nyquist criterion (see Section 6.4) to a particular class of nonlinear closed-loop systems.

Equation (9.49a) can be rearranged into the form

$$G(j\omega) = \frac{-1}{DF(E)} \tag{9.49b}$$

Equation (9.49b) can be solved graphically by plotting $G(j\omega)$ on the Nyquist plane, and determining the values of E and ω at which $G(j\omega)$ and $-1/DF(E)$, which is represented by a line running along part of the real axis, intersect.

9.4.2 Application: Periodic Breathing with Apnea

To illustrate a specific application of the describing function method, we turn to the model of Cheyne–Stokes breathing discussed in Section 6.7. As one might recall, this was a linearized model. However, for our present purposes, we will introduce a *thresholding nonlinearity* into the model by assuming that the controller output will become zero once the operating level of P_{aCO_2} falls below a certain value, B. In other words, the simulated episodes of Cheyne–Stokes breathing would include periods of apnea. A schematic block diagram of this model is shown in Figure 9.19a, and examples of the waveforms in P_{aCO_2} and V_E that one would expect to find are displayed in Figure 9.19b.

For simplicity, in the current example we will assume that there is only one chemoreflex loop in the system and that, unlike the example considered in Section 6.7, the controller responds instantaneously to changes in P_{aCO_2}. Suppose the controller response is given by

$$\begin{aligned} \dot{V}_E &= S_{CO_2}(P_{aCO_2} - B), & P_{aCO_2} > B \\ &= 0, & P_{aCO_2} \leq B \end{aligned} \tag{9.50}$$

where S_{CO_2} is the slope of the steady state ventilatory response to CO_2. We assume also that during periodic breathing, the P_{aCO_2} waveform can be characterized by

$$P_{aCO_2} = A \sin\theta + P_M \tag{9.51}$$

where $\theta = \omega t$ and P_M represents the mean level of the arterial P_{CO_2} signal. Substituting Equation (9.51) into Equation (9.50), we obtain

$$\begin{aligned} \dot{V}_E &= S_{CO_2}(A \sin\theta + P_M - B), & 0 < \theta < \theta_1 \text{ or } \theta_2 < \theta < 2\pi \\ &= 0, & \theta_1 \leq \theta \leq \theta_2 \end{aligned} \tag{9.52}$$

where θ_1 and θ_2 represent the two points in the periodic breathing cycle at which P_{aCO_2} crosses the apneic threshold, B (see Figure 9.19b). Thus, θ_1 and θ_2 can be computed from Equation (9.51):

$$\theta_{1,2} = \sin^{-1}\left(\frac{B - P_M}{A}\right) \tag{9.53}$$

If we assume, as illustrated in Figure 9.19b, that $B < P_M$, then $\sin\theta_1 < 0$, implying that θ_1 will be in the third quadrant ($\pi < \theta_1 < 3\pi/2$). If we define

$$\theta_0 = \sin^{-1}\left(\frac{|B - P_M|}{A}\right) \tag{9.54}$$

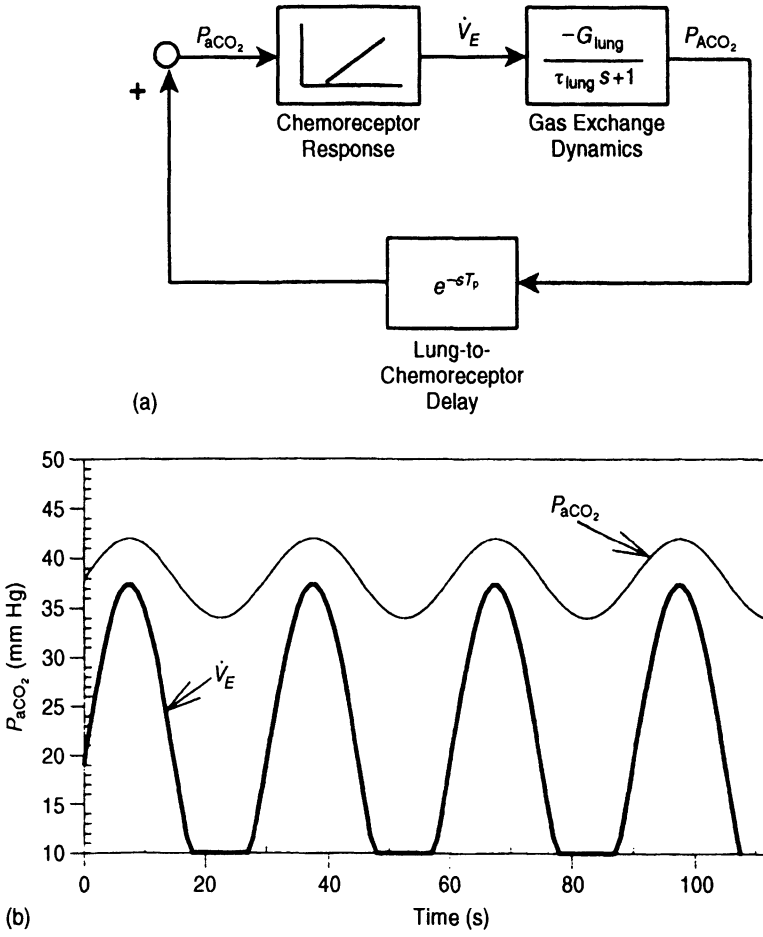

Figure 9.19 (a) Model of periodic breathing with apnea. (b) Input (P_{aCO_2}) to and output (V_E) from the thresholding nonlinearity.

so that $0 < \theta_0 < \pi/2$, then

$$\theta_1 = \pi + \theta_0 \qquad \text{and} \qquad \theta_2 = 2\pi - \theta_0 \tag{9.55a,b}$$

We know from the previous section that, since Equation (9.50) is a single-valued function, the imaginary part (b_1) of DF must equal zero. In order to evaluate the real part, a_1, we substitute the expressions in Equation (9.52) and (9.55a,b) into Equation (9.43) to obtain

$$\begin{aligned} a_1 &= \frac{1}{\pi}\left(\int_0^{\theta_1} S_{CO_2}(A\sin\theta + P_M - B)\sin\theta\, d\theta + \int_{\theta_2}^{2\pi} S_{CO_2}(A\sin\theta + P_M - b)\sin\theta\, d\theta\right) \\ &= -\frac{S_{CO_2}A}{2\pi}\left(\pi + 2\theta_0 - \sin 2\theta_0 + \frac{4(P_M - B)}{A}\cos\theta_0\right) \end{aligned} \tag{9.56}$$

Therefore, the describing function of the nonlinear chemoreceptor characteristic is

$$DF(A) = \frac{S_{CO_2}}{2\pi}\left(\pi + 2\theta_0 - \sin 2\theta_0 = \frac{4(P_M - B)}{A}\cos\theta_0\right) \tag{9.57}$$

where θ_0 is determined from Equation (9.54). The linear dynamic portion of this model (see Figure 9.19b and Section 6.7) is characterized by the following frequency response:

$$G(j\omega) = \frac{G_{lung}}{(1 + j\omega\tau_{lung})} e^{-j\omega T_d} \tag{9.58}$$

where T_d represents the lung-to-chemoreceptor delay, and G_{lung} and τ_{lung} were defined in Equations (6.45) and (6.46).

The existence of a limit cycle is predicted if the locus of $G(j\omega)$ on the Nyquist plane intersects with the locus defined by $-1/DF(A)$. Figure 9.20 shows the solution obtained using MATLAB m-file, `df_resp.m` for the case of a patient with congestive heart failure. As in Section 6.7, the parameter values used to represent this type of subject were $V_{lung} = 2.5$ L, $K_{CO_2} = 0.0065$ mm Hg^{-1}, $\dot{V}_E = 0.12$ L s^{-1}, $\dot{V}_D = 0.03$ L s^{-1}, $P_{ICO_2} = 0$, $P_{aCO_2} = P_{ACO_2} = 40$ mm Hg, $Q = 0.05$ L s^{-1}, $B = 37$ mm Hg, and $S_{CO_2} = 0.02$ L s^{-1} mm Hg^{-1}. Using Equations (6.45) and (6.46), it can be determined that these parameters produce values for G_{lung} and τ_{lung} of 108 mm Hg s L^{-1} and 6.75 s, respectively. The circulatory delay (T_D) employed was 14.2 s. Since the function $-1/DF(A)$ consists only of real values, its locus merely retraces a portion of the real axis. The point at which the two functions intersect (indicated by the open circle in Figure 9.20) corresponds to a frequency of 0.026 Hz, which translates into a periodicity of 38.5 s. This point also yields a value of 9.95 mm Hg for the amplitude of the oscillation in P_{aCO_2}. This calculation was undertaken merely to illustrate how the describing function method can be applied. As a predictor, it grossly underestimates the periodicity associated with Cheyne–Stokes breathing since it does not take into account the contributions of both chemoreflex loops and also ignores the response time associated with the chemoreflex. Incorporating these factors would produce

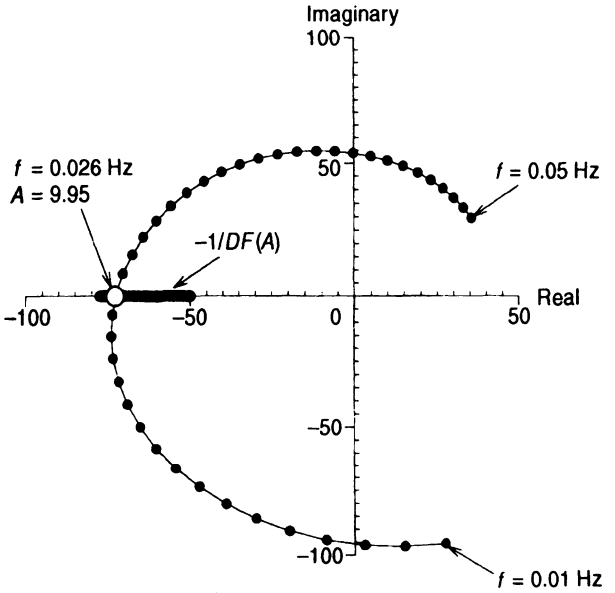

Figure 9.20 Illustration of the describing function method for determining the periodicity and amplitude of Cheyne–Stokes breathing in congestive heart failure. Thick line on real axis represents the locus of the functions $-1/DF(A)$. Intersection of this locus with that of the linear transfer function $G(j\omega)$ yields solution for limit cycle.

more realistic predictions, but would make the expression for $G(j\omega)$ much more complicated.

9.5 MODELS OF NEURONAL DYNAMICS

We saw in Section 9.3 the utility of employing the van der Pol and Poincaré models as theoretical constructs for characterizing the dynamic behavior observed in physiological oscillators, such as cardiac and circadian pacemakers. However, they represent only the class of systems that are spontaneously oscillating. There is an even larger class of systems that do not spontaneously oscillate, but which can oscillate given sufficient stimulation. These systems provide a better description of the properties of nerve and muscle tissue. As the following discussion will show, these models may be viewed as closed-loop systems with both negative and positive feedback.

9.5.1 The Hodgkin–Huxley Model

The first relatively complete mathematical model of neuronal membrane dynamics was published by Hodgkin and Huxley in 1952. This work laid the foundation for further development of a quantitative approach to understanding the biophysical mechanism of action potential generation and was the seminal achievement that won them the Nobel Prize in 1963. Their model was based largely on empirical findings obtained through application of the voltage-clamp technique, which we discussed briefly in Section 7.4.4. This melding of physical intuition, modeling principles, and excellent experimental design is a classic example of first-class bioengineering research.

Under resting conditions, the intracellular space of the nerve cell is on the order of 60 mV more negative relative to the extracellular fluid. This net equilibrium potential is determined by the ionic concentration gradients across the slightly permeable membrane as well as by effect of active transport by the sodium–potassium pump. There is a higher concentration of potassium ions inside the cell versus a higher concentration of sodium and chloride ions on the outside. However, the membrane permeabilities to sodium and potassium are strongly dependent on the membrane potential. Depolarization of the membrane potential leads to rapid changes in sodium permeability and a somewhat slower time-course in potassium permeability. The Hodgkin–Huxley model postulates that it is the initial rapid influx of sodium ions and the subsequent outflow of potassium ions that account for the generation of the action potential that follows the depolarizing stimulus. The chloride ions do not play much of a role but account primarily for a small leakage current into the cell. The electrical circuit analog of this model is displayed in Figure 9.21a. E_K, E_{Na} and E_{Cl} represent the Nernst potentials for potassium, sodium, and chloride, respectively. Based on their measurements on the squid giant axon, Hodgkin and Huxley employed values of -12, 115 and 10.6 mV for E_K, E_{Na}, and E_{Cl}, respectively. (It should be noted that they assumed the membrane potential difference to be measured outside relative to inside; thus, their sign convention was opposite to what has generally been adopted since their early work.) C represents the membrane capacitance, which is on the order of 1 μF cm^{-2}. g_K, g_{Na}, and g_{Cl} represent the respective conductances for potassium, sodium, and chloride ions that correspond to the resistive elements displayed in Figure 9.21a; because of their voltage dependence, g_K and g_{Na} have been shown as variable resistors.

Application of Kirchhoff's law to the circuit in Figure 9.21a yields the following equation relating the total membrane current I to the potential difference V across the membrane:

$$I = C\frac{dV}{dt} + g_k(V - E_k) + g_{Na}(V - E_{Na}) + g_{Cl}(V - E_{Cl}) \tag{9.59}$$

The dependence of g_{Na} on membrane voltage is characterized by the following expressions:

$$g_{Na} = G_{Na}m^3h \tag{9.60}$$

where G_{Na} is a constant and assigned the value of 120 millimho cm^{-2} by Hodgkin and Huxley. The time-course of g_{Na} is assumed to be the result of interaction between two processes, one represented by the "activation" state variable, m, and the other by the "inactivation" state variable, h, where m and h each may vary from 0 to 1. These state variables each obey first-order dynamics:

$$\frac{dm}{dt} = \alpha_m(1 - m) - \beta_m m \tag{9.61}$$

and

$$\frac{dh}{dt} = \alpha_h(1 - h) - \beta_h h \tag{9.62}$$

where the rate "constants" are voltage-dependent quantities defined by the following:

$$\alpha_m = (0.1(25 - V)(e^{(25-V)/10} - 1)^{-1} \tag{9.63}$$

$$\beta_m = 0.125e^{-V/80} \tag{9.64}$$

$$\alpha_h = 0.07e^{-V/20} \tag{9.65}$$

$$\beta_h = 1/(e^{(30-V)/10} - 1) \tag{9.66}$$

The potassium conductance follows similar but somewhat simpler dynamics:

$$g_K = G_K n^4 \tag{9.67}$$

where G_K is constant and given the value of 36 millimho cm^{-2} in Hodgkin and Huxley's simulations. The single state variable, n, is assumed to obey the following first-order differential equation:

$$\frac{dn}{dt} = \alpha_n(1 - n) - \beta_n n \tag{9.68}$$

where

$$\alpha_n = 0.01(10 - V)(e^{(10-V)/10} - 1)^{-1} \tag{9.69}$$

and

$$\beta_n = 0.125e^{-V/80} \tag{9.70}$$

Finally, the membrane conductance for chloride ions is assumed to be constant and equal to 0.3 millimho cm^{-2}.

Equations (9.59) through (9.70) constitute the Hodgkin–Huxley model. Functionally, the dynamic behavior represented by this set of equations can also be modeled in terms of the closed-loop system shown in Figure 9.21b. A depolarizing stimulus that exceeds the threshold produces an increase in sodium conductance, which allows sodium ions to enter the

intracellular space. This leads to further depolarization and greater increase in sodium conductance. This positive feedback effect is responsible for the rising phase of the action potential. However, fortunately, there is a built-in inactivation mechanism (represented by h) that now begins to reverse the depolarization process. This reversal is aided by the negative feedback effect of the increase in potassium conductance, which follows a time-course slower than that of the sodium conductance. The outflow of potassium ions leads to further repolarization of the membrane potential. Thus, the action potential is now in its declining phase. Because the potassium conductance remains above its resting level even after sodium conductance has returned to equilibrium, the nerve cell continues to be slightly hyperpolarized for a few more milliseconds following the end of the action potential. Figure 9.22, reproduced from the original Hodgkin–Huxley paper, shows the time-courses for V, g_{Na}, and g_K as predicted by the model to occur during an action potential. The curve labeled g represents the time-course of the overall membrane conductance. Multiplying this function with V allows us to predict the time-course for the net membrane current during the action potential.

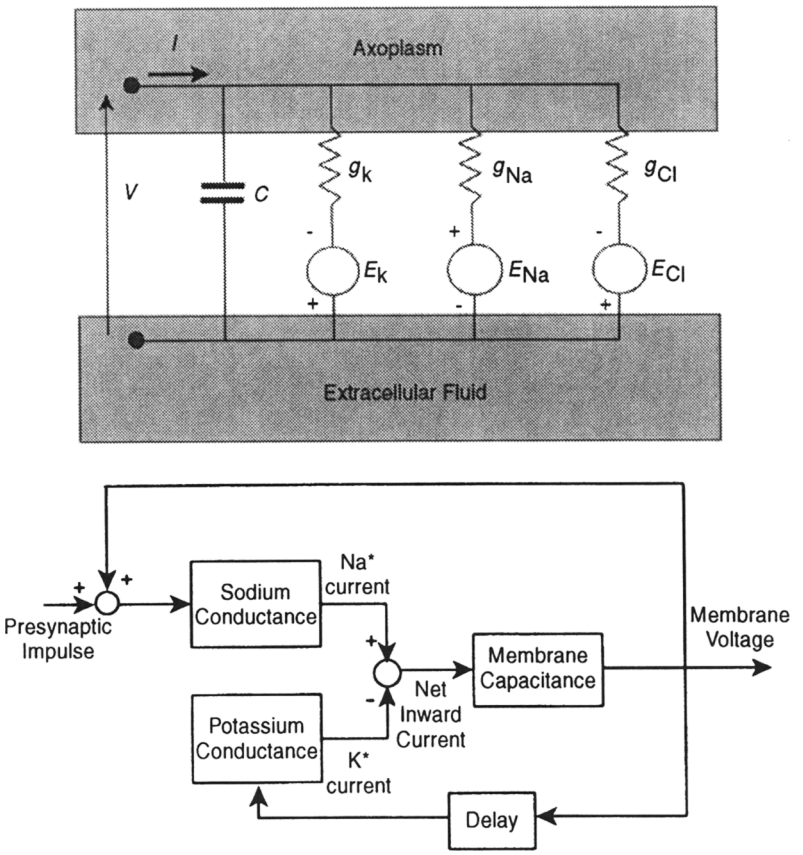

Figure 9.21 (a) Circuit analog of the Hodgkin–Huxley nerve membrane model. (b) The Hodgkin–Huxley model as a closed-loop system with negative and positive feedback.

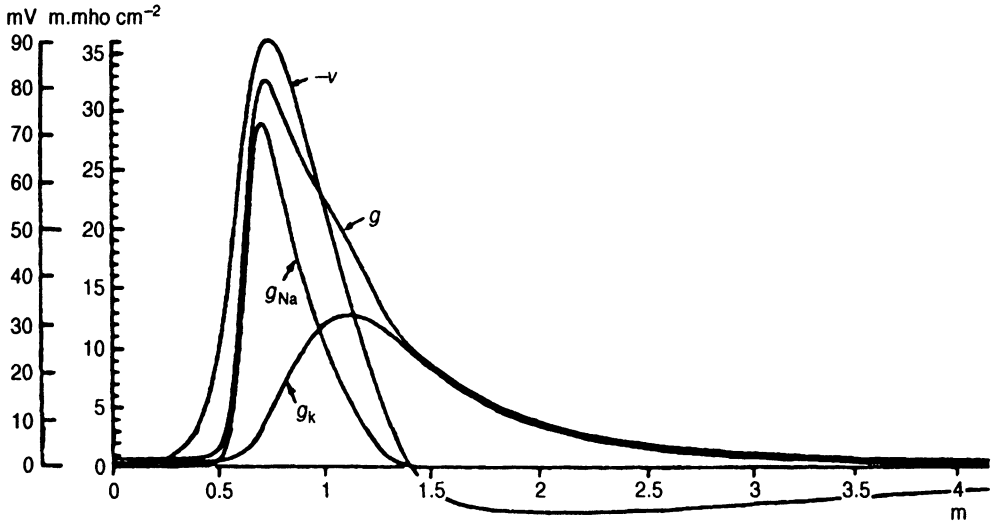

Figure 9.22 Time-courses of ionic conductances and membrane potential during an action potential, as predicted by numerical solution of the Hodgkin–Huxley equations. Membrane voltage is displayed as predominantly negative because Hodgkin and Huxley referenced all voltages to the intracellular fluid. (Reproduced from Hodgkin and Huxley, 1952).

9.5.2 The Bonhoeffer–van der Pol Model

Although the Hodgkin–Huxley equation set is able to reproduce many features of neuronal dynamics, it constitutes a somewhat unwieldy model, containing several state variables and a large number of empirical constants. Fitzhugh (1961) considered the Bonhoeffer–van der Pol (BvP) model as a simplified alternative, demonstrating the similarity of the phase-space characteristics of the former to the reduced phase-space behavior of the Hodgkin–Huxley model. The differential equations representing the BvP model are very similar to those of the van der Pol, which was discussed in Section 9.3.2. These are

$$\frac{dx}{dt} = c\left(y - \frac{x^3}{3} + x + z\right) \tag{9.71}$$

and

$$\frac{dy}{dt} = -\frac{1}{c}(x - a + by) \tag{9.72}$$

where a, b, and c are constants that satisfy the following constraints:

$$1 - \frac{2b}{3} < a < 1 \tag{9.73}$$

$$0 < b < 1 \tag{9.74}$$

$$b < c^2 \tag{9.75}$$

The variable z in Equation (9.71) represents the magnitude of the stimulus applied to the model. This can consist of two components. The first is the steady-state level of the stimulus (i.e., z = constant); as we will demonstrate below, since this enters into Equation (9.71)

explicitly, it can change the dynamics of the model quite dramatically. The second component of z is the transient contribution, which generally takes the form of a brief pulse of given magnitude.

By setting dx/dt and dy/dt in Equations (9.71) and (9.72) to zero, we can obtain expressions for the x- and y-nullclines, respectively. The x-nullcline is given by the cubic equation

$$y = \frac{x^3}{3} - x - z \tag{9.76}$$

which is the same as the x-nullcline for the van der Pol model except that, here, the vertical position (in phase space) of the cubic curve is controlled by the stimulus level (z). The y-nullcline is given by

$$y = \frac{(a - x)}{b} \tag{9.77}$$

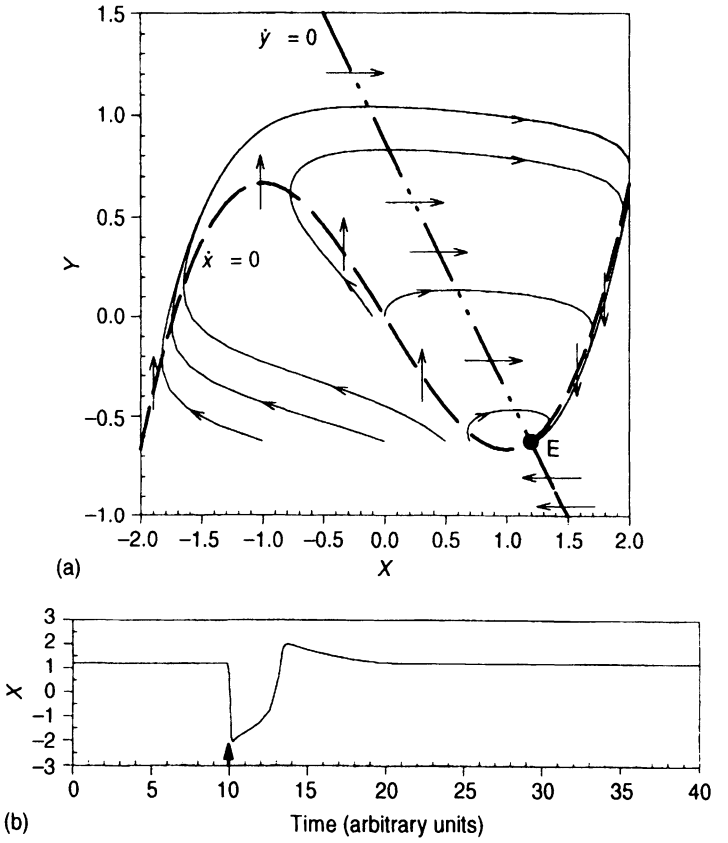

Figure 9.23 (a) Phase-plane diagram of the Bonhoeffer–van der Pol model with steady-state stimulus level (z) set equal to zero. Bold dashed curve represents x-nullcline ($dx/dt = 0$, vertical arrows); bold chained line represents y-nullcline ($dy/dt = 0$, horizontal arrows). Other curves are sample phase trajectories. E is the stable singular point; $a = 0.7$, $b = 0.8$, and $c = 3$ (b) Time response of BvP model to impulsive disturbance delivered at $t = 10$ (bold arrow).

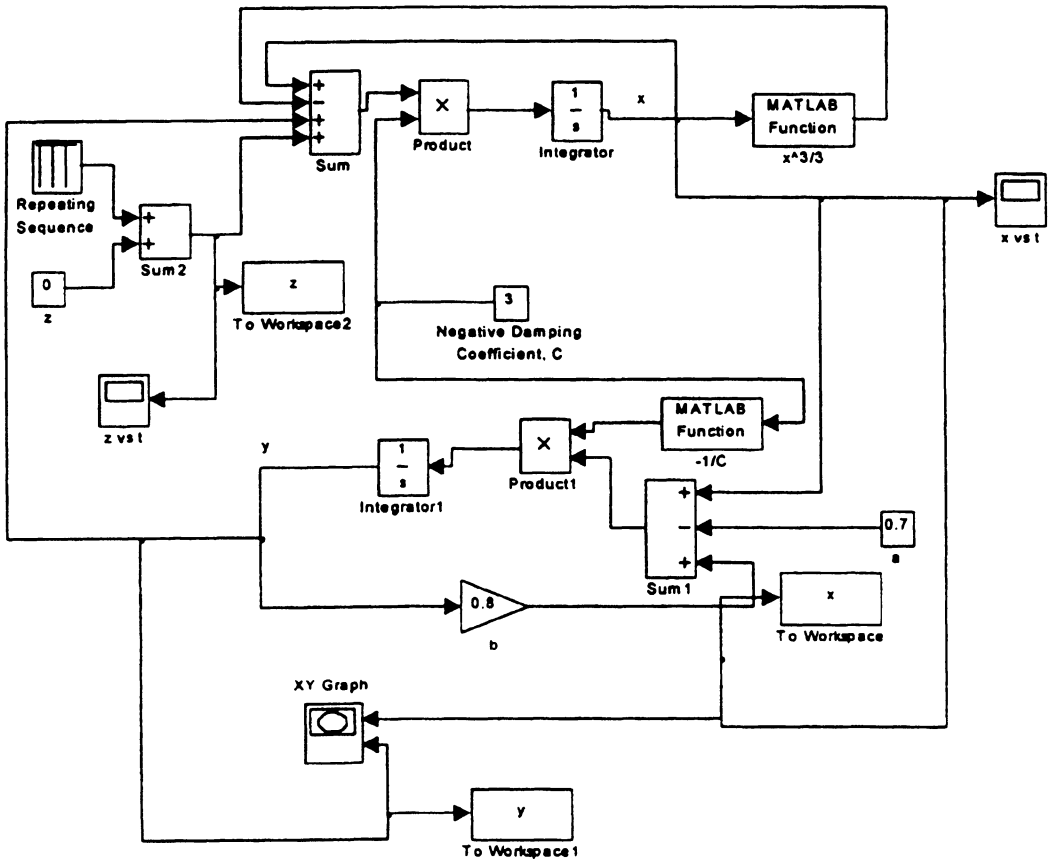

Figure 9.24 SIMULINK implementation ("bvpmod.mdl") of the Bonhoeffer–van der Pol model for parameter values $c = 3$, $a = 0.7$, and $b = 0.8$. x represents membrane voltage (with inverted sign), while z represents the applied stimulus, which includes a constant level plus instantaneous impulses applied at times specified in the repeating sequence block.

which is a straight line with negative slope. The conditions specified in Equations (9.73) through (9.75) guarantee that there will be only one intersection between the two nullclines. An example of the phase plane diagram for $a = 0.7$, $b = 0.8$, $c = 3$, and $z = 0$ is displayed in Figure 9.23a. In this case, the single equilibrium point is located at coordinates $x = 1.2$ and $y = -0.625$ (point E in Figure 9.23a). This singular point may be shown, using the analysis technique of Section 9.2.1, to be a stable focus. To the left of the y-nullcline ($y < (a - x)/b$), evaluation of Equation (9.72) shows that dy/dt must be positive. Thus, the trajectories that cross the x-nullcline in this region must be directed upward. Conversely, in the region to the right of the y-nullcline, the trajectories that cross the x-nullcline must point downward. In the region above the x-nullcline, evaluation of Equation (9.71) shows that dx/dt is positive and therefore, the horizontal arrows on the y-nullcline in this region must be directed rightward. By similar reasoning, the trajectories that cross the y-nullcline below the x-nullcline must be directed leftward. Thus, the general flow is in a clockwise direction, as shown in Figure 9.23a.

The time-course of x, which simulates membrane voltage, for one of the sample phase trajectories is displayed in Figure 9.23b. Application of a brief pulse of magnitude ($\Delta z =$) -5

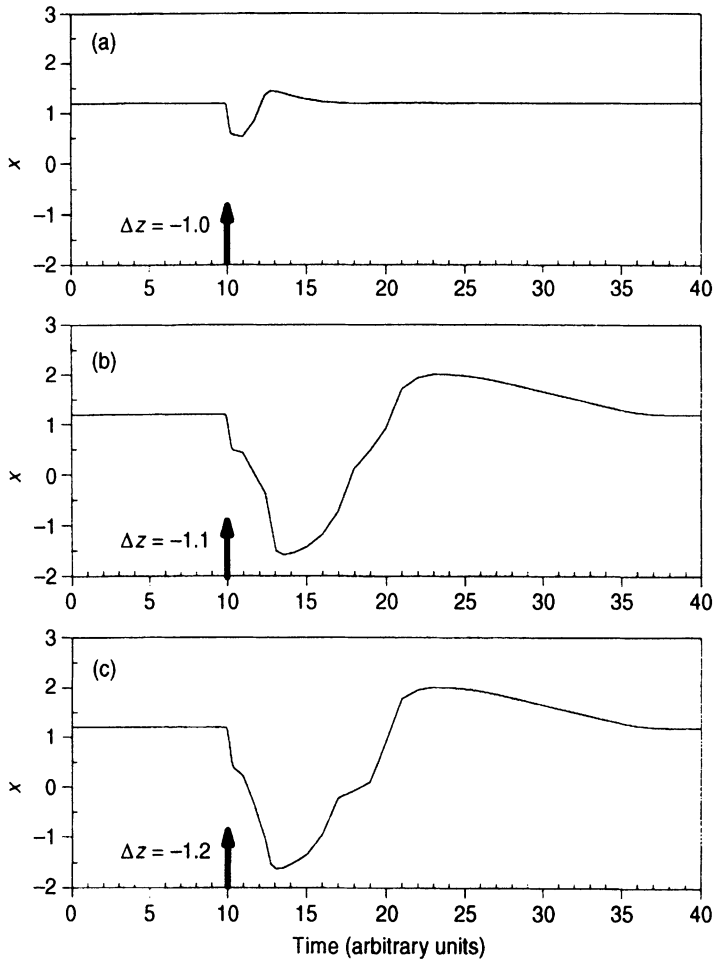

Figure 9.25 Demonstration of the threshold property of the Bonhoeffer–van der Pol model. Brief pulses of magnitudes −1.0 (a), −1.1 (b) and −1.2 (c) are applied through the variable z (baseline level of $z = 0$) at $t = 10$. Only the latter two cases are suprathreshold and produce "action potentials."

units at time $t = 10$ produces an abrupt decrease in x, followed later by a more gradual recovery, a small overshoot, and finally a slow return to baseline. Thus, this pattern of x simulates an inverted action potential (compare this to Figure 9.22). For this reason, we will refer to negative changes in x or z as "depolarizing" and positive changes as "repolarizing." The simulation result shown in Figure 9.23b and others that are displayed in subsequent figures were produced by a SIMULINK implementation of the BvP model, named "`bvpmod.mdl`." The diagram of the SIMULINK configuration for this model is shown in Figure 9.24. A "repeating sequence" block is used to generate the brief "shocks" (pulses in z) that are applied to the model. It should be noted from Figure 9.23a that, in general, only negative pulses in z (if sufficiently strong) would generate action potentials, since these displace the state point to the left of the equilibrium point.

One basic property of nerve and muscle tissue is the "all or none" phenomenon of thresholding. A pulse of insufficient magnitude, when applied to the nerve or muscle cell,

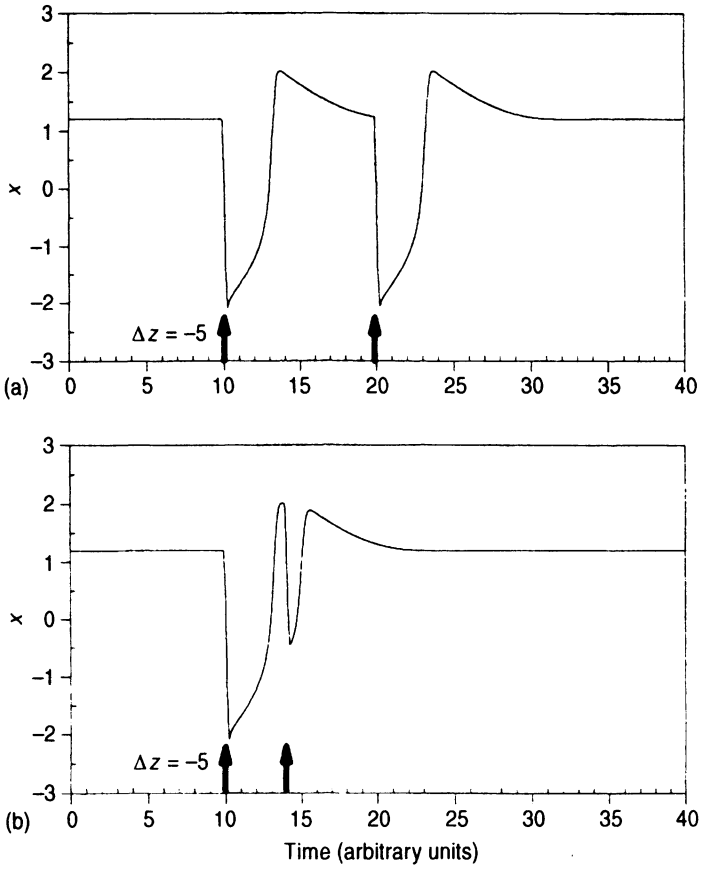

Figure 9.26 Demonstration of the refractory property of the Bonhoeffer–van der Pol model. (a) Brief pulses of magnitude -5 applied at $t = 10$ and $t = 20$ produce separate "action potentials"; (b) The brief pulse applied at $t = 10$ produces an action potential, but the succeeding pulse at $t \sim 14$, during the "refractory interval," does not.

produces only a small "depolarization" but does not elicit a full-fledged action potential. However, if the stimulus magnitude is increased above threshold, the action potential becomes unstoppable. The BvP model shows this type of behavior, as illustrated in Figure 9.25. In Figure 9.25a, a brief pulse of magnitude -1.0 produces only subthreshold behavior— a small and brief depolarization before x returns to baseline. In the phase-plane diagram, this is represented by a small displacement of the state point to the left of the equilibrium point, E. As long as the displaced state point falls to the right of the negatively-sloped portion of the x-nullcline or not too far to the left of it, the resulting phase trajectory will follow a small loop that leads back into E. However, if the pulse is large enough to push the state point sufficiently leftward of the x-nullcline, the subsequent phase trajectory will be one that moves leftward and upward, turns to the right, and then moves back toward E. The corresponding time-course of x would be the action potential displayed in Figure 9.25b. Increasing the stimulus pulse magnitude does not alter the size of the action potential, as shown in Figure 9.25c and Figure 9.23a.

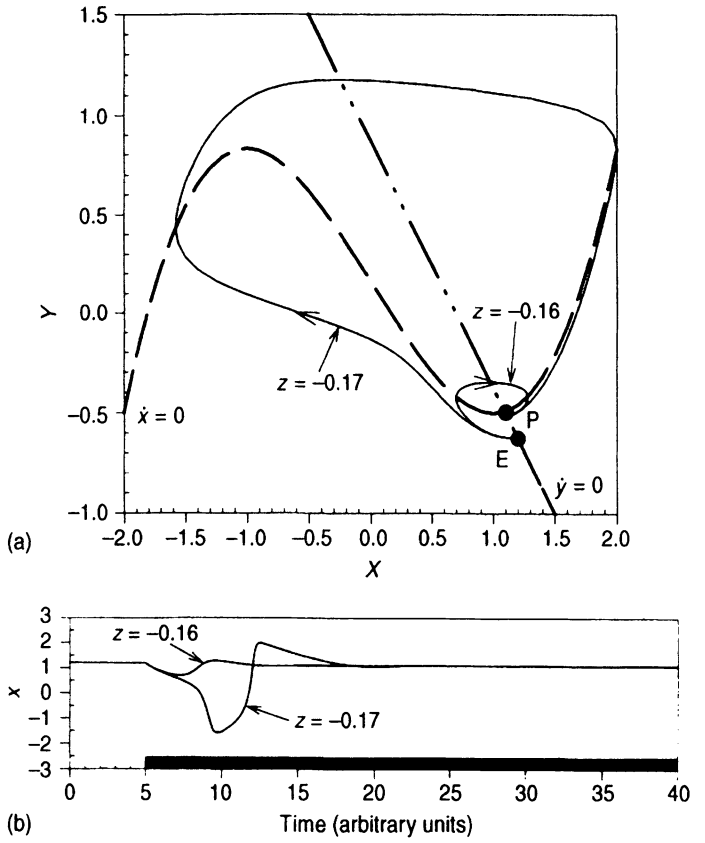

Figure 9.27 Responses of the Bonhoeffer–van der Pol model to "step depolarizations." (a) Phase-plane diagram showing the change in singular point from E to P following application of step in z of -0.16 units. The resulting response in x is subthreshold. When the step is made slightly more negative ($z = -0.17$), an action potential is generated. The singular point corresponding to $z = -0.17$ is located very close to P and therefore is not shown separately. (b) Time-courses of x following step depolarizations applied at $t = 5$ (indicated by black horizontal bar).

Another fundamental neuronal property is the presence of a refractory period. If a depolarizing stimulus is applied to a nerve cell too soon after the firing of an action potential, this stimulus will not elicit another action potential. The BvP model also exhibits this kind of behavior. Figure 9.26a shows the effect of stimulating the BvP model with two brief pulses of magnitude -5 units, spaced 10 time units apart. The second pulse occurs after much of the response to the first pulse has already taken place. Consequently, this second pulse leads to another action potential. In Figure 9.26b, the second pulse is applied only 4 time units after the application of the first pulse. This occurs during the early stages of the "repolarization." The net result is a small and brief depolarization, but a second action potential does not take place. This behavior can be better understood if one turns again to the phase-plane diagram in Figure 9.23. It can be seen that any stimulus that displaces the state point horizontally to the left (negative Δz) when the latter is on the final two portions of the phase trajectory, will not change its subsequent movement much, because the state point will basically follow its original course back toward E.

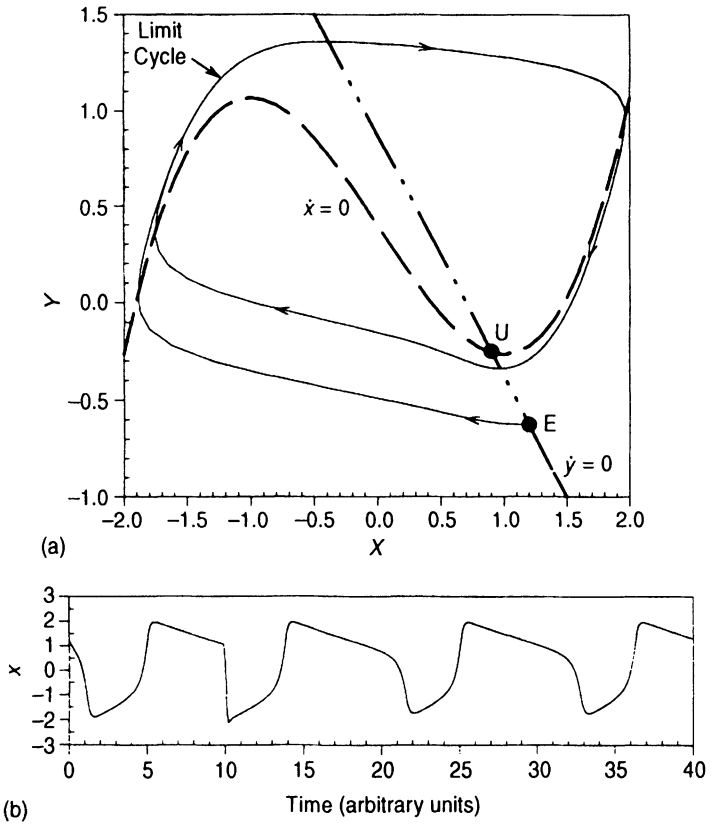

Figure 9.28 Conditions that lead to a train of "action potentials" from the Bonhoeffer–van der Pol model. (a) Simulating a "step depolarization" by setting $z = -0.4$ shifts the x-nullcline upward and produces a new unstable singular point (U). The net result is the creation of a stable limit cycle that encloses the unstable focus. (b) Time-course of x during application of depolarizing step.

Thus far, we have examined how the BvP model responds to brief pulses in z. What is the effect of changing the baseline level of z, which until now has been assumed to equal zero? From Equation (9.76), it is clear that giving z a nonzero value would shift the vertical position of the x-nullcline: positive z-values would move the cubic curve downward, while negative z-values, corresponding to step depolarizations, would move it upward. Figure 9.27 shows how the model would respond when subjected to step changes in z from zero to -0.16 and -0.17. In the phase-plane diagram (Figure 9.27a), the state-point starts off at E, prior to application of the step stimulus. When the step is applied, the x-nullcline moves upward so that the new singular point (labeled P) is now located at $x = 1.1$ and $y = -0.5$. The resulting response in x, however, is subthreshold (Figure 9.27b), and the corresponding phase trajectory is a small loop that begins at E and ends at P (Figure 9.27a). If the step in z is made only slightly more negative ($z = -0.17$), the response becomes quite different. Now, the phase trajectory that describes the dynamics of x between $z = 0$ and $z = -0.17$ takes the form of the large loop that corresponds to the generation of an action potential (Figure 9.27b). In both cases, the new singular points remain stable. Consequently, following the occurrence of the action potential, the state variable, x, settles down to a new steady level. However, when the

applied steps in z are made sufficiently negative, in addition to being displaced further upward, the new singular point (U) also becomes unstable (Figure 9.28). Instead of converging to the new "equilibrium" level, x simply oscillates around it (Figure 9.28b). In the phase-plane diagram (Figure 9.28a), this corresponds to the phase trajectory that begins at E but eventually gets trapped in the limit cycle that encloses the unstable focus, U. Thus, the BvP model predicts that when sufficiently large step depolarizations are applied, an infinite periodic train of action potentials will be generated. However, both BvP and Hodgkin–Huxley models are not able to simulate finite trains of action potentials, a phenomenon commonly observed in experimental nerve preparations.

BIBLIOGRAPHY

Bahill, A.T. *Bioengineering: Biomedical, Medical and Clinical Engineering*. Prentice-Hall, Englewood Cliffs, NJ, 1981.

Fitzhugh, R. Impulses and physiological states in theoretical models of nerve membrane. *Biophys. J.* **1**: 445–466, 1961.

Friedland, B. *Advanced Control System Design*. Prentice-Hall, New York, 1996.

Guevara, M.R., and L. Glass. Phase-locking, period doubling bifurcations and chaos in a mathematical model of a periodically driven oscillator: a theory for the entrainment of biological oscillators and the generation of cardiac dysrhythmias. *Math. Biology* **14**: 1–23, 1982.

Hodgkin, A.L., and A.F. Huxley. A quantitative description of membrane current and its application to conduction and excitation in nerve. *J. Physiol. (Lond.)* **117**: 500–544, 1952.

Kaplan, D., and L. Glass. *Understanding Nonlinear Dynamics*. Springer-Verlag, New York, 1995.

Korta, L.B., J.D. Horgan, and R.L. Lange. Stability analysis of the human respiratory system. *Proc. Natl. Electronics Conf.*, vol. 21, 1965; pp. 201–206.

Pavlidis, T. *Biological Oscillators: Their Mathematical Analysis*. Academic Press, New York, 1973.

Talbot, S.A., and U. Gessner. *Systems Physiology*. Wiley, New York, 1973.

Thompson, J.M.T., and H.B. Stewart. *Nonlinear Dynamics and Chaos*. Wiley, New York, 1986.

van der Pol, B., and J. van der Mark. The heartbeat considered as a relaxation oscillation, and an electrical model of the heart. *Phil. Mag.* **6**: 763–775, 1928.

PROBLEMS

P9.1. Consider the dynamical system defined by the following pair of coupled first-order differential equations:

$$\frac{dx}{dt} = x - \frac{x^3}{3} + y - 1.5$$
$$\frac{dy}{dt} = \frac{1 - 0.6x - 0.48y}{5.4}$$

Sketch the phase-plane diagram for this system, showing the x- and y-nullclines, as well as the general directions of flow for the phase trajectories. Find out where the singular point in this system is located and determine its stability characteristics.

P9.2 The regulation of the populations of two competing animal species, X and Y, can be modeled approximately by assuming the following pair of coupled differential equations:

$$\frac{dx}{dt} = (a - bx - cy)x$$

$$\frac{dy}{dt} = (e - fx - gy)y$$

where x and y represent the populations of X and Y, respectively, and a, b, c, d, e, f, and g are all positive constants. Note from each equation that the rate of population growth of either species increases directly with the current population, but as the population becomes progressively larger relative to the availability of food, there will be a tendency for starvation to decrease the rate of growth (quadratic terms in x or y). Furthermore, since the two species compete for the same limited food supply, a larger population of Y would inhibit the population growth of X and vice versa (cross-product terms). Depending on the values of the constants, stable populations of X and Y might coexist or one species might out-survive the other. Determine what would be the likely outcomes for these two species if:

(a) $\frac{a}{c} > \frac{e}{g}$ and $\frac{a}{b} > \frac{e}{f}$

(b) $\frac{a}{c} > \frac{e}{g}$ and $\frac{a}{b} < \frac{e}{f}$

(c) $\frac{a}{c} < \frac{e}{g}$ and $\frac{a}{b} < \frac{e}{f}$

(d) $\frac{a}{c} < \frac{e}{g}$ and $\frac{a}{b} > \frac{e}{f}$

P9.3. Develop the SIMULINK model of the system given in Problem P9.1. Determine the phase portrait of this dynamical system by computing the phase trajectories from several different starting locations on the phase plane.

P9.4. Use the describing function method to determine whether a limit cycle exists for the respiratory control model discussed in Section 9.4.2 if the controller response is characterized by the following equations:

$$\dot{V}_E = 0.02(P_{aCO_2} - 37), \qquad P_{aCO_2} > 39$$
$$= 0, \qquad P_{aCO_2} \leq 39$$

where $\dot{V}_E$ is given in units of L s^{-1}. This controller response function differs from that given in Equation (9.50) in that there is an abrupt silencing of chemoreceptor output when P_{aCO_2} is decreased from values slightly greater than 39 mm Hg to values below 39 mm Hg. Assume in your computations the values for the other parameters as given in Section 9.4.2. If a limit cycle exists, determine the periodicity and amplitude of the oscillation.

P9.5. In the example of describing function analysis given in Section 9.4.2, the predicted oscillation period for Cheyne–Stokes breathing was on the order of 40 s. This is substantially shorter than the ~60 s cycle-time that is more frequently observed. Determine whether the inclusion of additional factors, such as circulatory mixing and chemoreceptor response time, can account for much of the difference. To do this, extend the overall transfer function of the linear component so that it takes on the following frequency response:

$$G(j\omega) = \frac{G_{lung}}{(1 + j\omega\tau_{lung})(1 + j\omega\tau_{circ})(1 + j\omega\tau_{chemo})} e^{-j\omega T_d}$$

Assume that $\tau_{circ} = 2$ s and $\tau_{chemo} = 15$ s. For other parameters, use the values employed in Section 9.4.2.

P9.6. By decreasing the normalized period (T_s/T_0) of the stimulation from 0.95 to 0.5 in the SIMULINK program "`poincare.mdl`," explore the changes in the phase relationship between the stimulus and response changes in the Poincaré oscillator during type 1 resetting with the magnitude of the stimulus, b, set equal to 0.9.

P9.7. Derive Equation (9.38), which relates the old phase ϕ to the new phase θ of the Poincaré oscillator when it is perturbed by a single, isolated shock of magnitude b.

P9.8. Modify the SIMULINK implementation ("`vdpmod.mdl`") of the van der Pol model so that it can be driven by an external periodic stimulus of magnitude B and frequency f. Thus, modify this model so that its dynamics are described by Equations (9.33) and (9.34). First, set B equal to 2 and vary f in small increments from 0.01 to 0.2 Hz. Then, set B equal to 0.5 and vary f over the same range of frequencies. In each case, determine the band of frequencies over which entrainment occurs. Does the strength of the external forcing affect the entrainment band?

P9.9. Figure P9.1 shows the SIMULINK implementation ("`linhhmod.mdl`") of the linearized, closed-loop representation of the Hodgkin–Huxley model displayed in Figure 9.21b. Use this model to determine the membrane voltage response to a brief depolarization pulse of 60 mV. Does this model display the properties of thresholding and refractoriness? Modify the model to simulate voltage clamp experiments, in which the membrane voltage is constrained to follow a step change of +60 mV. Determine the time-courses of the sodium and potassium currents following the step depolarization.

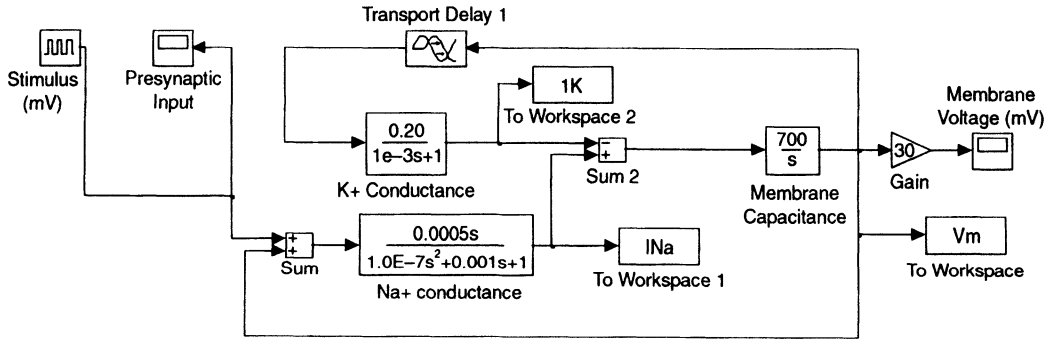

Figure P9.1 Linearized SIMULINK representation ("`linhhmod.mdl`") of the Hodgkin–Huxley model.